

**INTEGRATED OPTICAL FILTERS
BASED ON
MICRORING RESONATORS**

Freddy Tan

The research described in this thesis was carried out at the Integrated Optical MicroSystems (IOMS) Group, Faculty of Electrical Engineering, Mathematics and Computer Science, MESA⁺ Research Institute, University of Twente, P.O.Box 217, 7500 AE Enschede, The Netherlands.

This work was supported financially by the BTS project ringresonatoren (Senter) for the first two years and the last two years by the European Commission (EC) funded Information Society Technologies (IST) project Next-generation Active Integrated optic Subsystems (NAIS), with contract number IST-2000-28018.

Cover: Microscope picture of two parallel cascaded microring resonators at resonance obtained with an infrared CCD camera. The rings have a radius of 25 μm and a width of 2 μm and are realized in silicon nitride.

Copyright © 2004 by Freddy Susanto Tan, Enschede, The Netherlands

ISBN: 90 - 365 - 2023 - 1

**INTEGRATED OPTICAL FILTERS
BASED ON
MICRORING RESONATORS**

PROEFSCHRIFT

ter verkrijging van
de graad van doctor aan de Universiteit Twente,
op gezag van de rector magnificus,
prof. dr. F.A. van Vught,
volgens besluit van het College voor Promoties
in het openbaar te verdedigen
op vrijdag 20 februari 2004 om 13.15 uur

door

Freddy Susanto Tan

geboren op 24 november 1966

te Bandung, Indonesië

Dit proefschrift is goedgekeurd door:

De promotor Prof. Dr. A. Driessen

*This thesis is dedicated to
My father and the memory of my mother
My wife and children*

Contents

Chapter 1. Introduction	1
1.1 Optical communication	1
1.2 Optical filters in WDM systems	3
1.3 BTS project ringresonatoren	5
1.4 IST project Next-generation Active Integrated optics Subsystem (NAIS) project	6
1.5 Outline of the thesis	8
Chapter 2. General concepts of microring resonator devices	11
2.1 Microring resonator devices	11
2.2 Working principle of microring resonator devices	12
2.3 The lateral and vertical coupling configuration	15
2.3.1 The lateral coupling configuration	15
2.3.2 The vertical coupling configuration	16
2.4 Cascaded multiple microring resonator devices	17
2.4.1 Serial configuration	17
2.4.2 Parallel configuration	18
2.5 Performance of microring resonator devices	20
2.6 Characterization methods	23
Conclusions	25
Chapter 3. Design strategy	27
3.1 Input fields for the design activity	27
3.1.1 Knowledge	27
3.1.2 Previous experiences	29
3.1.3 Design tools	30
3.1.4 Technology and facilities	32
3.1.5 Objectives	33
3.1.6 Time frame	34

3.1.7 System specifications	34
3.2 Field of specific activities	35
3.2.1 Design	35
3.2.2 Realization	37
3.2.3 Intermediate characterization	37
3.2.4 Functional characterization	38
3.2.5 System demonstrator	39
Conclusions	39
Chapter 4. High finesse single-ring resonator devices based on a lateral coupling configuration for WDM applications	41
Chapter 5. Single microring resonator devices based on a vertical coupling configuration	47
5.1 Silicon Oxynitride based microring resonator devices	47
5.1.1 Design considerations	48
5.1.2 Fabrication process for the complete devices	49
5.1.3 Device performance	53
5.2 Characterization of vertically waveguide coupled microring resonators by means of quantitative image analysis	56
5.3 Silicon Nitride based microring resonator devices	64
5.3.1 Design considerations	64
5.3.2 Fabrication process for the complete devices	65
5.3.3 Device performance	66
5.3.4 High finesse vertically coupled waveguide-microring resonators based on $\text{Si}_3\text{N}_4\text{-SiO}_2$ technology	67
Conclusions	70

Chapter 6. Cascaded multiple microring resonators as optical bandpass filter	71
6.1 Design of cascaded multiple microring resonators in the parallel configuration	72
6.2 Fabrication process of cascaded multiple microring resonators in the parallel configuration	73
6.3 Simulation model of cascaded multiple microring resonators in the parallel configuration	75
6.4 Experimental results	76
Conclusions	80
Chapter 7. Compact spectral slicer devices based on microring resonators	81
7.1 Introduction	81
7.2 Design of compact spectral slicers based on vertically coupled microring resonators	81
7.3 Realization of the spectral slicer devices	87
7.4 Experimental results	87
Conclusions	90
Chapter 8. Summary and Recommendations	93
8.1 Summary	93
8.2 Recommendations	95
References	99
Publications	109
Acknowledgment	115
Curriculum Vitae	117

Chapter 1

Introduction

1.1 Optical communication

The invention of the laser in 1960 [Maiman 1960] made available a coherent (i.e. monochromatic) radiation source some $10^4 - 10^5$ times higher in frequency than the existing microwave generators with a frequency of about 10^{10} Hz. Since then much efforts has been spent to use the laser for communications. It was thought that a communication systems operating at optical frequencies would increase the information carrying capacity by as much as 100,000 times compared to the microwave systems existing at that time. Besides the light source also transmission lines were needed with low transmission loss to arrive eventually at optical communication systems.

In 1966, glass optical fibers had been considered as suitable and effective transmission lines but their losses were still high. In 1970, Kapron, et al. [Kapron 1970] from Corning Glass Works fabricated a silica fiber with an attenuation of 20 dB/km. At this attenuation level, the repeater spacing for optical fiber links becomes comparable to those of copper systems making the lightwave technology a practical alternative. In the next two decades, data transmission via optical fiber became more and more attractive because the attenuation of the optical fibers could be reduced below 0.2 dB/km in the 1550 nm wavelength window.

The devices that are employed in present day communication systems are a combination of electronic and optical technology. In long distance communication links, mostly optical fibers have been used and sophisticated devices have been developed with extremely high performance with respect to transmission speed, the number of wavelengths and the transmission distance.

As many users share the costs of these devices, bulk optics technology can be used with extremely good technical performance but very high cost. In short distance links, where only a few users can share the costs, mostly electronic devices are in use nevertheless their limited transmission capacity.

Nowadays, metropolitan networks are already optical and access networks are becoming more and more optical. The adaptation of solutions from long distance communications are probably not appropriate anymore for access

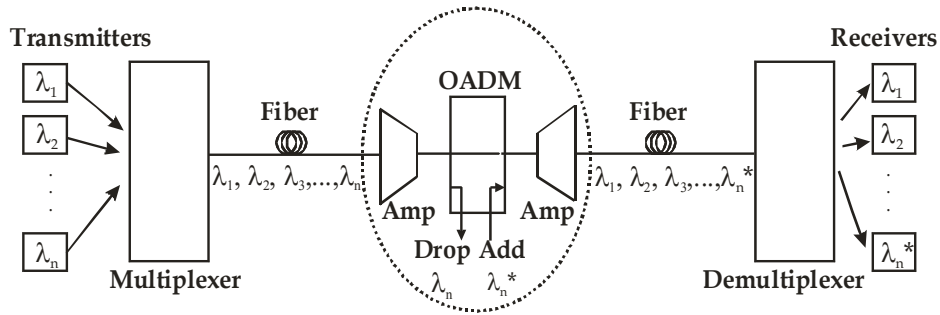


Fig. 1.1 Schematic layout of wavelength division multiplexing (WDM) systems

network where the single users are responsible for the cost by themselves. For the implementation in access network, one needs optical systems and devices, which operating at high bit rates ($> \text{Gbit/s}$) allow complex optical routing and data processing and are compact and low-cost without need of maintenance by trained engineers [Driessen 2003].

The rapid growth in demand for high-capacity telecommunication links and the speed limitation of electronics used in single-wavelength optical links have resulted in an extraordinary increase in the use of wavelength division multiplexing (WDM). A WDM system can multiply the transmission capacity of a single optical fiber link several times by multiplexing a large number of wavelengths and launch them into a single optical fiber.

Basic components in a point to point WDM connection are transmitters, multiplexer, optical fiber link with perhaps optical amplifiers, demultiplexers and receivers. For additional nodes in between, optical add-drop multiplexers (OADM) are necessary. This situation is schematically depicted in Fig. 1.1. At the transmitter side a WDM multiplexer connects the optical signals from N transmitters operating each at its own wavelength, λ_n to a single optical fiber. At the OADM, a signal of one or more specific wavelengths is dropped and new data on the same wavelengths are added. The signals arriving at the demultiplexer will be demultiplexed and each wavelength will be directed to one of the N receivers.

1.2 Optical filters in WDM systems

Optical filter in WDM systems can function for example as (de) multiplexer and add-drop components. There are several well-known devices that can be used as (de) multiplexer and add-drop filter such as the Arrayed Waveguide Grating (AWG) [Smit 1996], thin film filters, Bragg gratings, etc. These devices

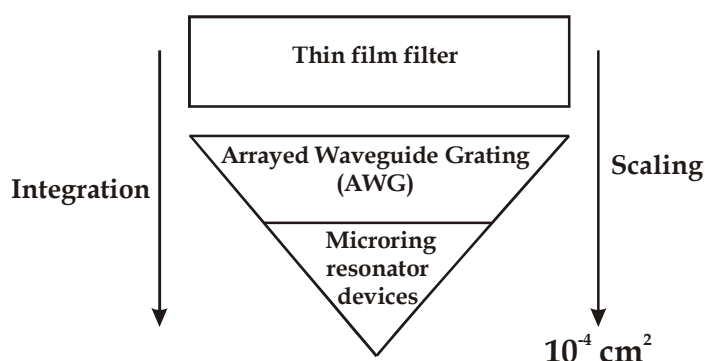


Fig. 1.2 Size reductions and integration capability of optical filter devices

are often relatively large and difficult to be integrated in compact devices with a rich functionality. Considering the success of highly integrated electronic structures fabricated in micro/nano system technology, it would be highly desirable to realize optical structures in a similar approach.

Integrated optical filters based on microring resonators can become as small as 10^{-4} cm² and could be promising functional elements in future large scale integrated photonics, see Fig.1.2. Compact optical filter devices based on microring resonators have been proposed since 1997 [Little 1997]. A cascaded six microring resonator device in a serial configuration (see also Sec. 2.4) has been announced on October 9, 2003 by Little Optics, Inc. [Little 2003].

There are three classes of microring resonator devices, which can be used in WDM applications. The first type is the microring resonator device with a Free Spectral Range (FSR) equal to the distance between WDM channels of about 10 - 100 GHz (0.08 nm - 0.8 nm). The second type is a filter with a FSR covering a large part of the WDM window that usually is related to the wavelength range of 1530 - 1560 nm where erbium doped fiber amplifiers (EDFA) are available. The third type is a microring based filter devices with a FSR larger than the standard WDM window, typically 50 nm - 100 nm.

The microring devices in the first category can be realized by using a moderate refractive index contrast material ($\Delta n \sim 0.05$) such as low index contrast SiON/SiO₂. They usually have a large radius of more than 300 μ m to be able to fit the FSR to the WDM channels. In this technology, conventional optical photolithography can be applied for fabrication. Fiber to chip coupling is usually not a problem because the straight waveguides have mode profiles that usually fit to the standard optical fiber. Relatively low refractive index contrast materials also mean lower scattering loss. Filters with a FSR of 50 GHz - 100 GHz and interleaver filter for 25 GHz spaced dense wavelength division multiplexing systems based on a serial cascaded microring resonator device (see also Sec. 2.4) have been realized by using this technology [Melloni 2003]. The second type of the microring devices can be fabricated by using a large refractive index contrast material ($\Delta n \sim 0.5$) such as high refractive index SiON or Si₃N₄ in combination with SiO₂. A typical bending radius is 10 μ m - 30 μ m, corresponding to a FSR of about 8 nm - 20 nm.

Also this technology allows conventional optical photolithography in the realization process. Therefore, the route to low-cost technology is feasible. Fiber to chip coupling becomes critical in this technology, but simple tapering sections and the use of small core fibers result in acceptable losses of a few tenths of dB.

The microring devices belonging to the third category can only be realized by using high refractive index contrast material ($\Delta n > 2$) such as Si/SiO₂ or III-V semiconductors and allow very small bend structure down to 2 μm – 5 μm . For these devices, conventional mask-based photolithography can not be used anymore. Only advanced deep UV techniques from the semiconductor industry or direct e-beam writing can be used to obtain acceptable performance. The propagation loss of these devices is relatively high (> 7 dB/cm) and mainly dominated by scattering loss due to the high refractive index contrast in the materials [Dumon 2003]. Fiber to chip coupling loss is usually very critical and becomes a problem in this technology.

This thesis presents devices consisting of single and parallel cascaded multiple microring resonators (see also Sec. 2.4), which belong to the second category that can be used as bandpass filters, spectral slicers and (de-) multiplexers. The results that are presented in this thesis have been obtained during the work within the framework of the BTS project “ringresonatoren” and the IST project “Next-generation Active Integrated optics Subsystem (NAIS)”.

1.3 BTS project ringresonatoren

The aim of the BTS project “ringresonatoren” was the realization of microring resonator devices, which can be used as an add-drop component in future DWDM telecommunication networks. There were 3 partners involved in this project founded by the Dutch Ministry of Economic Affairs: JDS Uniphase, BBV software BV, and the Integrated Optical MicroSystems (IOMS) Group (formerly Lightwave Devices Group).

In the first phase the studies have been based on a lateral coupling configuration. The material used for fabricating these devices was Low-Pressure Chemical Vapor Deposition (LPCVD) Silicon Nitride (Si_3N_4) with a refractive index of 1.98. This value was obtained by ellipsometric measurements and was extrapolated for a wavelength of 1550 nm. The devices have been designed to work for TE polarization to give sufficiently low bending loss.

Later on, the design of the microring resonator device has been based on the vertical coupling configuration. The LPCVD Si_3N_4 that has been used previously can not be used anymore for the microring core due to the requirement of polarization independence of the filter response. For the fabrication of these resonator devices, which can support only the fundamental TE and TM modes in vertical and radial directions Plasma Enhanced Chemical Vapor Deposition Silicon Oxynitride (PECVD SiON) with a refractive index of 1.65 has been chosen. It will be shown that it is difficult to obtain a polarization independent response with single microring resonator devices. By using a polarization diversity scheme, however, it is possible to make a wavelength selective polarization independent splitter, as has been proposed by Klunder et al. [Klunder 2002 (a)].

1.4 IST project Next-generation Active Integrated optics Subsystem (NAIS) project

The second project I have been involved in is the EC founded NAIS project, which has the objective to demonstrate the feasibility of a next generation compact integrated optics subsystem based on microring resonators as depicted in Fig. 1.4 [NAIS project]. In order to reach this objective, five technical Work Packages (WP's) have been considered in the project plan: materials research (WP 2), design activities (WP 3), technological realization (WP 4), characterization (WP 5) and system aspects (WP 6).

There are 12 partners involved in this EU project such as TUHH Technology GMBH, Nonlinear Optics Laboratory Institute of Quantum Electronics (ETH), Rainbow Photonics AG, Produits Chimiques Auxiliaires et de Synthese (PCAS), and Ecole Normale Superieure de Chemie de Montpllier (ENSCM), which are mainly dealing with materials to investigate the properties of new passive as well as organic electro-optic materials in WP 2. The Applied Analysis and Mathematical Physics (AAMP) Group of the University of

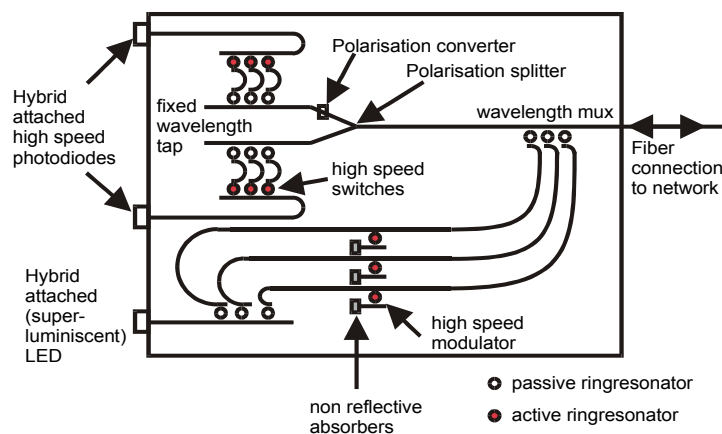


Fig. 1.4 Schematic layout of the transceiver on a single chip for an access network considered in the NAIS project

Twente, Concept to Volume (C2V) and the Institute of Radio Engineering and Electronics (IREE) are developing the simulation tools for designing active microresonators and complex integrated optics subsystems consisting of a large number of functional elements in WP 3. The Ecole Normale Superieure de Cachan (ENSC) is working on the fabrication and characterization of an active microring resonator in WP 4 and WP 5 and Universita degli Studi di Roma "La Sapienza" Dipartimento di Energitica is dealing with characterization of materials and devices in WP 5. Nortel Networks deals with the embedding of the subsystem in a network and the demands from the end-users in WP 6. Our own group, the Integrated Optical MicroSystems (IOMS) group is the coordinator and is involved in all of the WPs.

Within the NAIS project, the devices have been realized in the vertical coupling configuration. Single microring resonator devices made of LPCVD Si_3N_4 have been realized and demonstrated. Their drop response show narrow passbands, relatively low ON-OFF ratio (rejection ratio) and narrow stopbands due to the Lorentzian shape of the filter response obtained from the drop port. In order to improve the filter performance, parallel cascaded two- and three-ring resonator devices have been designed and realized in LPCVD Si_3N_4 technology. The wavelength response of these devices has shown a promising functionality as a bandpass filter as well as spectral slicer device.

1.5 Outline of the thesis

In the first phase of the present work, another Ph.D student, Dr. D.J.W Klunder was also dealing with microring resonator devices. In his work, devices with a lateral coupling configuration have been used [Klunder 2002 (b)]. The device information and basic theory already provided in that thesis is not repeated in this thesis.

This thesis deals with the design, fabrication and characterization of passive microring resonators devices. Chapter 1 gives an introduction to the development in optical communications. In addition, the projects where I had been involved are briefly presented. Chapter 2 introduces general concepts and relevant basic theory of optical microresonators and can be used as reference for the following chapters. Chapter 3 presents the design strategy for the realization of demonstrator devices. Chapter 4 presents the result of single microring resonator devices based on the lateral coupling configuration using LPCVD Si_3N_4 for the microring resonator core. A through response with a finesse of more than 100 has been demonstrated. Results on vertically coupled single microring resonators with a SiON (BTS) or Si_3N_4 (NAIS) core are discussed in Chapter 5. Chapter 6 presents the results of higher order filters. Parallel cascaded two- and three- microring resonator devices with equal coupling coefficient have been realized and demonstrated.

Chapter 7 discusses the feasibility of parallel cascaded microring resonators as compact spectral slicers with increased spectral efficiency. Chapter 8 gives a summary of this thesis and recommendations for future work.

Chapter 2

General concepts of microring resonator devices

In this chapter, general concepts and the relevant basic theory of microring resonators are presented. This includes also a discussion of the two possible coupling schemes i.e. the lateral and vertical coupling configuration. After a description of single resonator devices an analysis is given of the performance of multi-microring structures.

2.1 Microring resonator devices

The simplest configuration of a microring resonator device consists of one straight waveguide and one ring resonator. This device can be used as an all-pass filter [Madsen 1999] for applications as phase equalizer, dispersion compensator or optical delay line [Madsen 1999, Lenz].

Microring resonators as optical filters have attracted much attention due to their high wavelength selectivity [Blom 1997, Blom 1999, Little 1997, Little 1999] in combination with small size. They have also low on-chip insertion loss [Tan 2001 (b), Tan 2003 (b)]. Therefore they are potential candidates of very large scale integrated (VLSI) photonic circuits that could enable a device integration density of up to 10^5 devices per square centimeter [Chu 1999 (b), Little 2000 (a)].

In general, a microring resonator device functioning as an optical filter consists of two straight waveguide ports with a microring resonator in between, which can be arranged in a lateral or vertical coupling configuration as depicted in Fig. 2.1. Microring resonator devices can be composed by single ring or multiple rings (in serial or parallel configuration).

These devices can be used for diverse applications such as optical add-drop filters [Chin 1999, Chu 1999 (b), Ibrahim 2002, Little 1999, Suzuki 2002, Tan 2001 (a)], signal processing [Van 2002 (b)], switching [Blom 1997, Geuzebroek 2002, Ibrahim 2003, Little 1998, Van 2002 (a)], modulation [Abeles 2000,

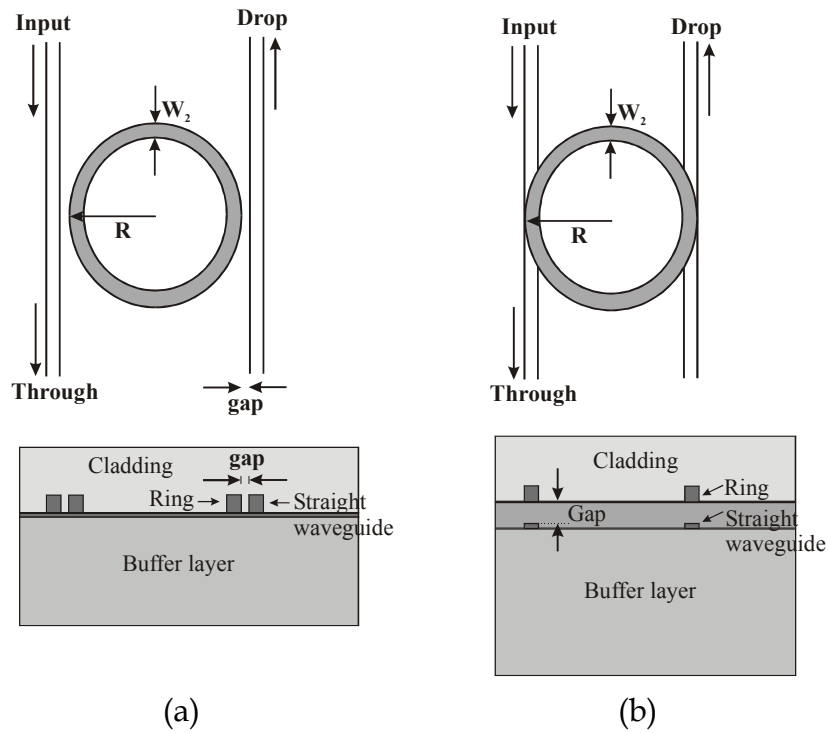


Fig. 2.1 Schematic layout of single microring resonator devices in top view and cross-section; (a) lateral coupling (b) vertical coupling configuration

Dapkus 2000, Rabiei 2002], wavelength conversion [Absil 2000], micro-laser [Levi 1993] and sensors [Heimala 1996, Krioukov 2002 (a), Krioukov 2002 (b), Krioukov 2003].

2.2 Working principle of microring resonator devices

Fig. 2.2 shows a single microring resonator device consisting of two straight waveguides functioning as input and output (drop) ports and the microring resonator with radius of R .

The performance of the device can conveniently be described by a set of parameters that include the propagation loss for a full roundtrip, α , and the field coupling coefficients and excess losses in the couplers, κ^n and χ^n respectively. Suppose that light is launched into the input port of the straight waveguide. A fraction κ^1 of the input field couples to the microring resonator and propagates along the ring, approximately $1-\kappa^1$ continues to the through port. At off-resonance, the fraction of the propagating field in the ring

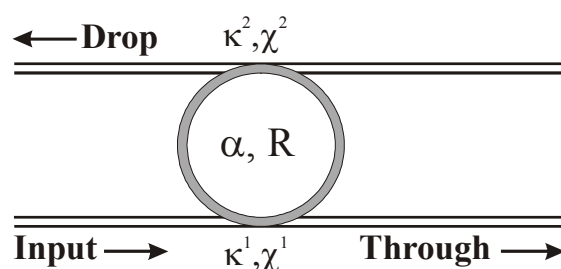


Fig. 2.2 Schematic layout of single microring resonator device with its device parameters (see text)

resonator, which has completed a single roundtrip, interferes destructively with the field just coupled to the ring. In this way no enhanced field amplitudes can be obtained inside the resonator. A part of the small field in the resonator is coupled back to the straight waveguide and leaves the through port. There it interferes with the field coming directly from the input. At resonance, the field inside the microring resonator interferes constructively with the field just coupled to the ring resulting in a coherent build-up of the field inside the microring resonator. A considerably fraction of power - in a loss-less resonator with equal couplers κ^1 and κ^2 100% - can in this case be coupled to the drop port. At the through port the field is largely reduced by the destructive interference between the fields directly coming from the input port and the part coupled from the enhanced field inside the resonator. A computer simulation tool has been made that allows the calculation of the resonator response based on the parameter given above.

On the other hand, by using the simulation model to fit experimental spectra obtained with a resonator, 'experimental' values for these parameters can be derived.

The coupling coefficients of the couplers are determined by the gap (g) between the straight waveguide and the microring resonator, the phasemismatch, Δn_{eff} (the effective refractive index difference between the straight waveguide and the microring resonator) and the relative position (s) of the center of the straight waveguide with respect to the position of the

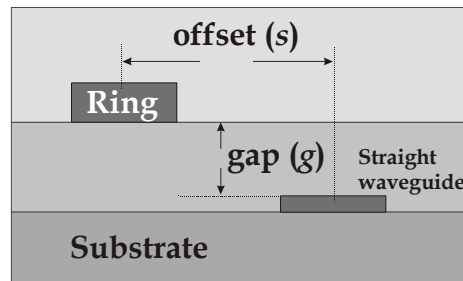


Fig. 2.3 Cross section of the coupling region in the vertical coupling configuration with its relevant parameters

center of the microring waveguide (offsets) in horizontal direction (see Fig. 2.3). The latter is relevant only for the vertical coupling configuration. Therefore, the coupling coefficient, κ^n can be tailored by choosing the appropriate parameters for the gap, the phasemismatch and the offset in horizontal direction. In our case, the coupler is modeled by directional couplers [Klunder 2002 (b)].

Several other coupling schemes have been introduced in the literature such as a multimode interference (MMI) coupler for the coupling region of a race track resonator with a radius of $100 \mu\text{m}$ and a length of the straight part of $150 \mu\text{m}$ for laser applications [Rabus 2001]. This device has a spectral response with a maximum FSR of 0.8 nm .

Race-track based directional couplers have been fabricated [Chin 1999] by using e-beam lithography in combination with deep etching using inductively coupled plasma reactive ion etching (ICP-RIE), where very small ring radius (cavity length of 31 μm , straight section in the coupling region of 6 μm) and very narrow gap down to 200 nm are allowed.

2.3 The lateral and vertical coupling configuration

In the following the two basic coupling schemes, lateral and vertical coupling will be discussed in detail. Also design aspects and fabrication issues will be presented.

2.3.1 The lateral coupling configuration

In the lateral coupling configuration for microring resonator devices the port waveguide(s) are structured in the same layer stack as the microresonator. Coupling then is controlled by the horizontal gap between microring and port waveguide (see Fig. 2.1a). The fabrication processes of this device can be made very simple as a single mask process can be applied. This configuration, however, misses flexibility as the straight waveguide and the microring resonator can not be optimized individually.

The main problem in the lateral coupling configuration is the precise structuring of the gap (see Fig. 2.1a) that depending on the materials system can vary between 150 -1000 nm with an accuracy needed of better than 10%. Conventional optical photolithography as applied in our case is only able to open a gap of 750 nm or more. A gap of 500 nm could not be opened even if we worked with a high-resolution e-beam mask for patterning. A good gap definition in the lateral coupling configuration therefore is rather difficult to be obtained. After our initial experiences with laterally coupled devices (see Ch. 3) we changed to the vertical coupling configuration (see Ch. 4).

The main reason for this is that the coupling now is determined for a large extent by the thickness of the separation layer, which can be deposited with accuracy better than 10 nm.

2.3.2 The vertical coupling configuration

In the vertical coupling configuration, the straight waveguides and the microring resonators are etched in different layers (see Fig. 2.1b). From the design point of view, this means increased flexibility because ring and port waveguides can be optimized separately. In practice, however, fabrication can experience severe difficulties due to possible misalignment between port waveguide and ring, especially if one uses the standard mask aligners (Karl Süss or EVG 620) that are available in the MESA⁺ clean room with a resolution not much better than 500 nm. A lot of effort and much attention have been put to minimize the misalignment problem. This problem can be solved only when a mask aligner with a higher resolution or a waferstepper become available.

In the vertical coupling configuration, the thickness of the port waveguide should be minimized to avoid planarization problems. By using a relatively high refractive index material such as LPCVD Si₃N₄ the thickness can be restricted to 140 nm. Another option is to apply Chemical Mechanical Polishing (CMP) to planarize the gap layer. This process, however, is rather difficult to be controlled on a nanometer scale, which results in a not well defined gap thickness.

The microring resonator core can be made of LPCVD Si₃N₄ that has a maximum thickness of approximately 300 nm or PECVD SiON with a 'maximum' refractive index of 1.65. The latter demands a thicker layer in the order of 1.5 μm because of its relatively low refractive index. A PECVD SiON layer with a refractive index of more than 1.65 is not recommended because it will introduce some technical problems such as contamination of the deposition chamber or, more important, cracking of the layer when an annealing step is applied [Albers 1995].

2.4 Cascaded multiple microring resonator devices

Microring resonator devices can consist of a single microring or cascaded multiple microrings in either the lateral or vertical coupling configuration. Fig. 2.2 shows a single microring resonator device in the vertical coupling configuration. These devices have shown promising functionality as filters (see also Ch. 4 and Ch. 5). A specially tailored filter response with an increased performance as needed in applications such as bandpass filter, spectral slicer, (de)multiplexer can be obtained by cascading multiple microring resonators and choosing the appropriate parameters (see also Ch. 6). Cascaded multiple ring resonator devices can be arranged in a serial or parallel configuration. In the following, both configurations will be discussed and explained in detail.

2.4.1 Serial configuration

Fig. 2.4 shows the schematic layout of cascaded multiple microring resonators in a serial configuration. Several microrings are positioned between the input and the output port of the straight waveguides. The coupling between the straight waveguides and the microring resonators and between two microring resonators is modeled by directional couplers with coupling coefficients, κ_n and excess losses in the coupler, χ_n . The propagation loss inside the microring resonator and the microring radius are indicated by α_n and R_n respectively.

Light is launched from the input port (see Fig. 2.4) and couples in part to the first microring. At off-resonance, the fraction of light, which has completed a single roundtrip, interferes destructively with the light that has just coupled to the ring. There is no build-up of the power inside the resonator. Only a small amount of light is coupled to the second ring. The light remains mainly in the straight waveguides and propagates to the through port. At on-resonance, the fraction of light that has just completed one roundtrip in the first ring, interferes constructively with the light that has just coupled to the ring resulting in a coherent build-up of the power inside the microring resonator.

A considerable fraction of power can be coupled to the second ring, and, after passing through all the microring resonators, is coupled finally to the drop port. All rings need to be at the same wavelength on resonance. Consequently a precise control of the fabrication process within nanometer precision is

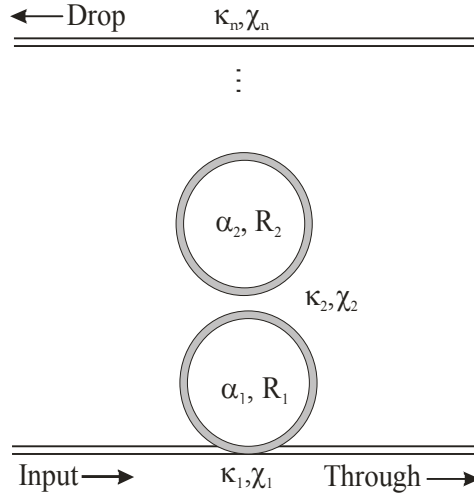


Fig. 2.4 Schematic layout of cascaded multiple microring resonators in serial configuration

necessary, for example, with regard to the ring radius. In addition, the direct interactions between two nearest neighbor rings ask for a technology with very limited fabrication tolerances. In order to tune the resonant wavelength of each microring resonator, special treatments are probably needed such as thermal tuning or UV trimming.

2.4.2 Parallel configuration

In the parallel configuration (see Fig. 2.5), the microrings are arranged in such a way that there is no direct interaction between the nearest neighbor rings but only an indirect one via the port waveguides. Therefore, the light propagates in a unique direction and consequently there is no counterpropagation.

The parallel configuration of multiple microring resonators offers more flexibility to the fabrication process compared to the serial configuration. The useful wavelength range of the microring resonator, however, is rather limited. The reason for this is the possible phase change occurring in the

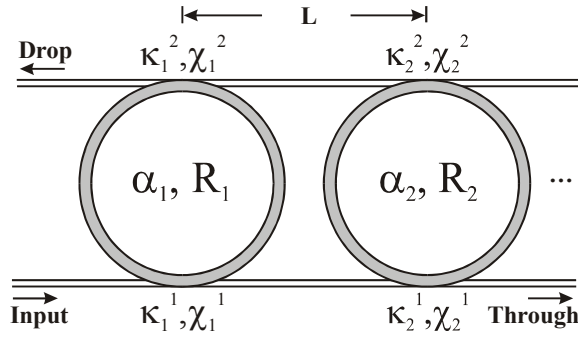


Fig. 2.5 Schematic layout of cascaded multiple microring resonators in the parallel configuration

connecting length, L between the microrings, which is optimized only for a narrow wavelength range. Outside this range the output of the drop port could largely vary in an undesired way due to the interference of light coming from the individual resonators.

The coupling between the straight waveguide and each microring resonator is taken into account by directional couplers. Each microring resonator with an effective refractive index, $n_{eff,ring}$ has the following parameters: coupling coefficient, κ_m^n , excess loss in the coupler, χ_m^n , propagation loss in the ring, α_m and ring radius, R_m . The distance of centre to centre between the nearest neighbor rings, L also determines the filter response. Therefore, this distance should be chosen carefully to obtain the desired interference at the specified wavelength range. By assuming that each microring is identical this distance can be determined by using the formula

$$L = \frac{m\lambda_c}{2n_{eff,sw}} \quad (2.1)$$

In this formula, m is an integer, λ_c is the resonant wavelength, and $n_{eff,sw}$ is the effective refractive index of the straight waveguides. When optimizing the filter design for the desired wavelength response, L should be varied just as any of the other parameters. Besides enabling the proper phase relation, the distance L should be set to be large enough to avoid any direct interaction between the neighboring rings.

2.5 Performance of microring resonator devices

The microring resonator devices have similar spectral response of the through- and the drop port for both, the lateral and the vertical coupling

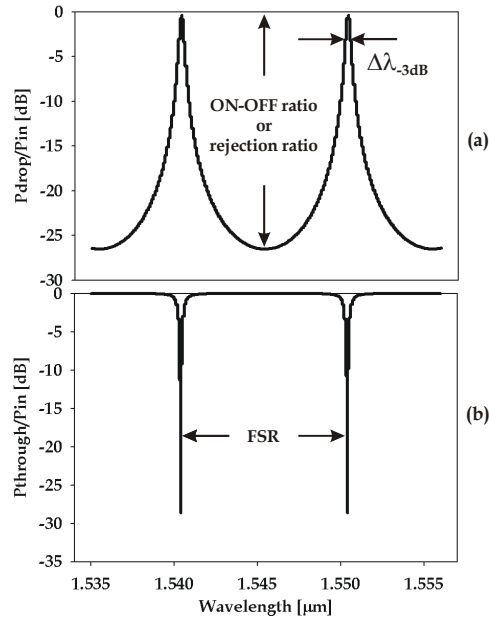


Fig. 2.6 Calculated spectral response of a single ring resonator device with a radius of $25 \mu\text{m}$; (a) drop response, (b) through response. The coupling coefficients, $\kappa^1 = \kappa^2 = 0.3$, $\alpha = 2 \text{ dB/cm}$ and $F = 32$

configuration (see Fig. 2.1). Fig. 2.6 shows the calculated spectral responses of the through- and drop- port (see Fig. 2.2) of a single-ring resonator as a function of wavelength.

By assuming that there is no coupling loss, the modal amplitude at the through port and the drop port of a single-ring device are given by the following expressions:

$$\frac{A_{through}}{A_{input}} = t_0^{(1)} - \sum_{q=1}^{\max} \frac{a_q}{b_q \exp(-jk_q(\lambda - \lambda_c)) - 1} \quad (2.2)$$

and

$$\frac{A_{drop}}{A_{input}} = - \sum_{q=1}^{\max} \frac{a_q}{b_q \exp(-jk_q(\lambda - \lambda_c)) - 1} \quad (2.3)$$

where λ_c is a central wavelength, k_q is related to the FSR by $k_q = 2\pi/\text{FSR}_q$; ρ is the roundtrip phase shift, q is the mode number of the radial ring resonator modes; $t_0^{(1)}$ is related to the coupled fraction between straight waveguide and ring resonator modes at the input straight waveguide; a_q and a_q' are related to the coupled fields and b_q represents a phase term. The detailed derivation of these equations and full definition of parameters can be found in [Klunder 2002 (b)]. The free spectral range, FSR is given by

$$FSR = \frac{\lambda_c^2}{2\pi N_{eff} R_{eff}} \quad (2.4)$$

where λ_c is the resonant wavelength, N_{eff} is the effective refractive index of the microring resonator mode, and R_{eff} is the effective radius of the microring resonator mode. The finesse of the resonator, F , is defined by the following relation

$$F = \frac{FSR}{\Delta\lambda_{-3dB}} \quad (2.5)$$

where $\Delta\lambda_{-3dB}$ is the bandwidth at -3 dB.

Specific properties of a single microresonator device such as the ON-OFF ratio, the bandwidth, etc. can be tailored mainly via the choice of the coupling coefficients and propagation loss inside the microring resonator [Tan 2003 (c)]. The device performance such as higher ON-OFF ratio and sharper roll-off can largely be improved by cascading several microring resonators as shown in Fig. 2.7. Also a flatter passband can be obtained by using this configuration [Kokubun 2002, Tan 2003 (e)].

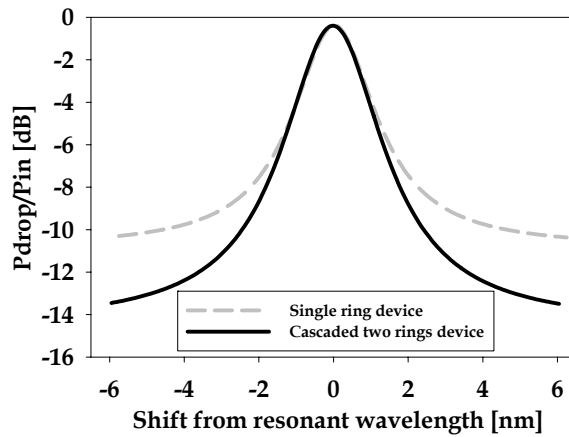


Fig. 2.7 Calculated spectral responses of a single ring and cascaded two rings devices with a radius of $20 \mu\text{m}$ that gives a FSR of about 10 nm and a finesse of about 5

With regard to the polarization dependence, the geometry of the microring and the material birefringence can cause a shift in the resonant wavelength for TE and TM polarization because the bend structure gives different effective refractive indices for TE and TM bend modes (see Eq. 5.1) even if there is no birefringence in the material. By careful design, selection of appropriate materials and applying UV-trimming nearly polarization independent devices can be realized [Chu 1999 (a)].

2.6 Characterization methods

Two methods have been used for the characterization of the devices: the standard measurement method and quantitative image analysis. In both approaches, a characterization set-up as shown in Fig. 2.8 is used. A tunable laser HP 8168C with a wavelength range between 1470 nm and 1580 nm and a

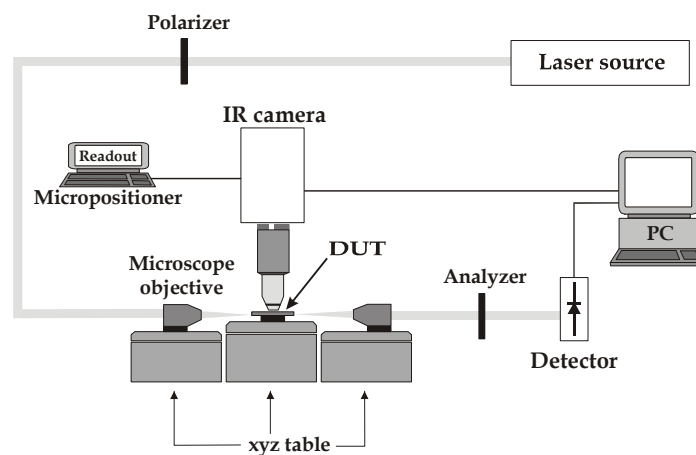


Fig. 2.8 Set up used for characterization of the devices by using the standard measurement and quantitative image analysis, DUT: device under test

spectral linewidth of 4 pm is used as a light source. The laser can be controlled by a computer to be able to perform a wavelength scan with a smallest stepsize of 1 pm. Characterization of the devices have been done by injecting the light to the input port of the device using a microscope objective (end-fire coupling). A polarizer determines the polarization state the incoming light, a second polarizer is used as an analyzer at the output side. The standard method is used to measure the global spectral response of the device by collecting the output, i.e. the through or drop port of the device by a microscope objective and projecting it to a detector connected to a computer.

Quantitative image analysis is used for on-chip measurement with a high spatial resolution. In this approach light scattered from the device is projected to an infrared (IR) camera (SU320M-1.7RT Indium Gallium Arsenide MiniCamera) by using a lens system to produce a magnified image.

The image sensor consists of a 320×240 pixel array with a pitch of $40 \mu\text{m}$. Fig. 2.9 shows an example of a high resolution picture of a microring at resonance with a magnification at the sensor array of about 130 times obtained with a microscope objective with $40 \times$ magnification and $\text{NA} = 0.75$. The ring radius is

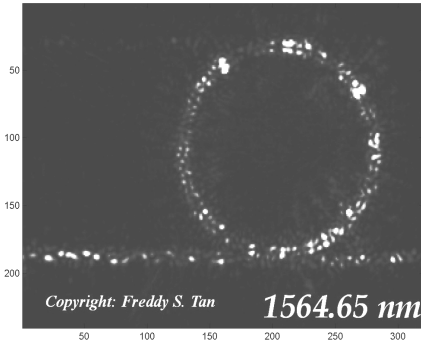


Fig. 2.9 High resolution picture of a ring resonator at resonance with a radius of $25 \mu\text{m}$ and a width of $2.5 \mu\text{m}$ magnified 130 times

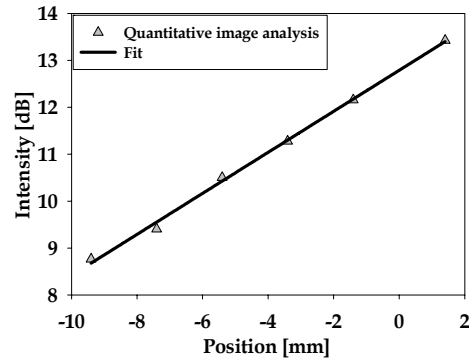


Fig. 2.10 Propagation loss of a straight waveguide obtained by quantitative image analysis

$25 \mu\text{m}$ and the width is $2.5 \mu\text{m}$. The method is based on the assumption that the light scattered from local scatter centers in the guiding layers and at interfaces is proportional to the local field intensity.

Image-processing software is used to process the images for deriving the important physical parameters of the device such as local intensity as a function of wavelength, propagation loss in the straight waveguide, on-chip insertion loss, on-chip drop efficiency etc. For waveguide loss measurements or large area inspections the scattered power within a defined small area is measured together with the relative position of each image. For this the movement of the IR camera is controlled by a calibrated micropositioner. Fig. 2.10 gives as an example propagation loss measurements of a straight waveguide at 1550 nm with resulting loss of $4.4 \pm 0.1 \text{ dB/cm}$.

Conclusions

Microring resonators are promising devices that offer high wavelength selectivity in combination with an extremely small size that enables an integration density of up to 10^5 devices per square centimeter.

Single and multiple microring devices can be implemented in structures where the port waveguides are laterally or alternatively vertically coupled to the microrings. For our applications and with the current technological equipment the vertical coupling configuration is the best choice as only in this configuration the straight waveguide and ring resonator can be optimized individually. Besides that, in the fabrication process, vertical coupling is more tolerant to the variation in technology than lateral coupling.

In the case of cascaded devices, the parallel configuration is more attractive than serial one as the filter response obtained from the drop port can be adjusted by varying the centre to centre distance of the nearest neighbor rings. Two characterization methods have been used to evaluate the performance of our devices, the standard measurement method that can be used for global spectral measurements at the port waveguides and quantitative images analysis. The latter provides precise information on the local light intensity at any place of the device with a spatial resolution of better than $2\ \mu\text{m}$ and a spectral resolution determined by the linewidth of the tunable laser source (4 pm).

Chapter 3

Design strategy

The general goal of this thesis is to elaborate new microresonator based optical filter structures resulting in a realistic design and eventually to realize demonstrator devices. In order to reach these objectives a design strategy has been set up, see Fig. 3.1. It is a complex scheme with a number of input fields to the design, intermediate action boxes, the final demonstrator device and many interaction lines that include feedback at any of the intermediate stages. In the following this scheme will be explained in some detail.

3.1 Input fields for the design activity

Before starting with the actual design activity the objectives, available knowledge and facilities and other boundary conditions have to be analyzed. Also the position of the devices in a communication system has to be considered.

3.1.1 Knowledge

The first input field for the design is related to the knowledge base available to this work composed by open literature and own understanding obtained in our group or in collaboration with partners. At the beginning of the project described in this thesis only a few groups were working in microring resonator devices that were pioneered by Blom et al. [Blom 1996, Blom 1997] and Little in 1997 [Little 1997]. Since that time, a lot of studies have been carried out not only theoretically and numerically but also experimentally for diverse applications. Also the number of groups working in this field has largely been enhanced.

Each group is working on a peculiar class of devices as, depending on the application, ring resonators can be realized in diverse materials systems such as low refractive index contrast SiON/SiO₂, high refractive index SiON or

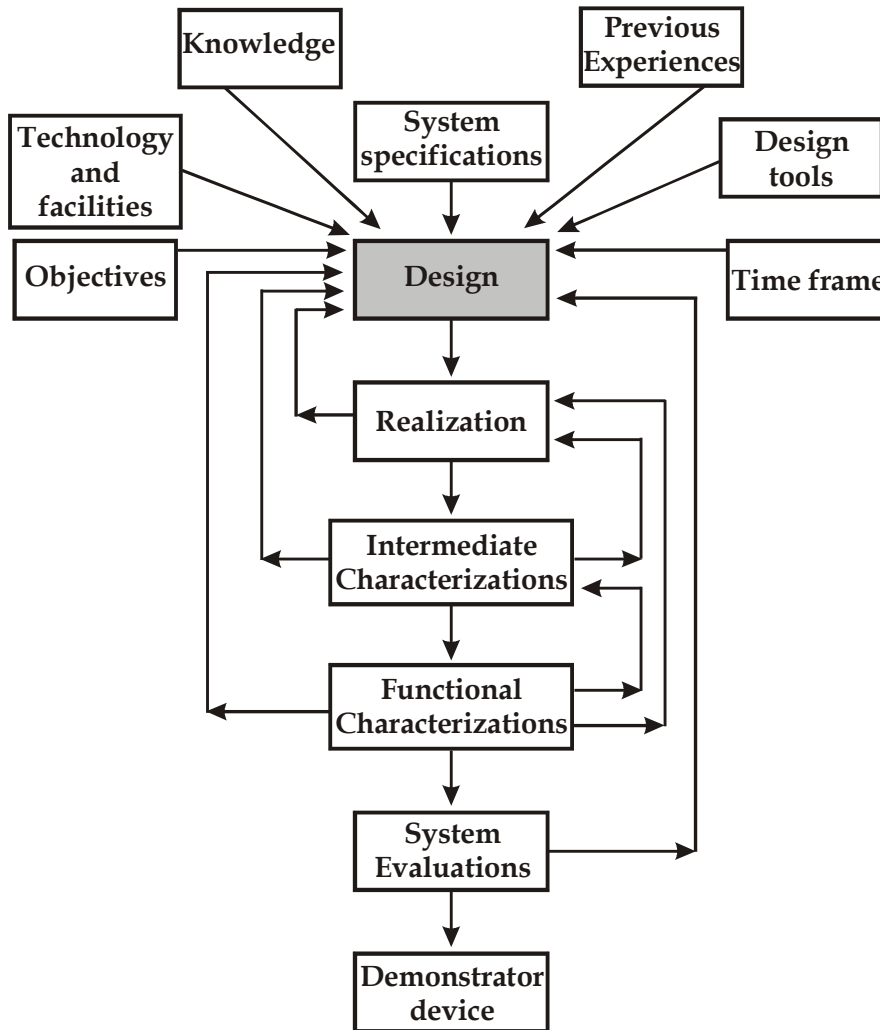


Fig. 3.1 General design strategy to achieve the objectives of the project

Si₃N₄ in combination with SiO₂ substrate, glass compound Ta₂O₅/SiO₂ and very high refractive index contrast material like Si/SiO₂ or III-V semiconductors.

In our group, high refractive index SiON or Si₃N₄ based structures in combination with SiO₂ substrates have been used. In a different project at the IOMS group also polymer based devices for electro-optic modulation are being developed [Leinse 2003]. In the course of the current study the knowledge basis has largely increased. This is reflected among others in the increasing complexity and performance of the devices like the spectral slicers of chapter 7. A good overview demonstrating the current status in the field has been presented in a recent Summerschool at Erice organized by the NAIS project [Bertolotti 2004]. The presentations of the invited talks can be found at the NAIS Website [NAIS Website].

3.1.2 Previous experiences

Probably the most important input field for the design activities is the previous experience that, being in certain aspects a specific subset of “knowledge”, exceeds it largely. It includes the many unwritten rules and unpublished and not for publication suitable results obtained by own effort or by informal discussion. In this respect, transfer of knowledge from previous PhD students in our group who were also working in the field of microresonators is the most important contribution. The first PhD student who had been working in this field is F. Blom (1996-1998). He has introduced as a pioneer the microresonator in our group and was one of the first with a publication on a working device [Blom 1998, Blom 1997]. His objective was to demonstrate all-optical switching by field enhancement. Disk and ring resonators have been realized with Si₃N₄/SiO₂ technology in combination with AKZO-DANS polymer by using a very basic technology. The results were promising, but all-optical switching could not be demonstrated experimentally. In a collaboration with another MESA⁺ group extended scanning nearfield optical microscopy (SNOM) pictures of one of his devices could be obtained revealing a rich spectrum of optical phenomena [Balistreri 2001, Klunder 2000 (a)].

A second PhD student at IOMS who was working in the field had been D.J.W Klunder (1998-2002) who explored experimentally and theoretically high finesse microresonators, mainly made in $\text{Si}_3\text{N}_4/\text{SiO}_2$ technology. In collaborations within IOMS and other MESA⁺ groups and later also with the NAIS project he deepened the understanding of microresonators and worked on new applications in the field of optical communication, optical sensing and stimulated emission. Another Ph.D student, C.G.H. Roeloffzen (1998-2002) had been working on optical filters for WDM applications on the basis of SiON waveguides that included relatively small FSR ring resonators.

The national BTS project (1999-2001) resulted in valuable experience for ring resonator devices for application in WDM networks. With the European NAIS project (2001-2004) the number of people involved was largely extended and progress has been made in all fields relevant for the successful realization of microring devices, see Ch. 1 for more detail. The experience accumulated at the end of this project and thereafter being available to the current design activities has augmented largely. As a consequence tasks that only a few years ago were considered to be very challenging are meanwhile routinely carried out.

3.1.3 Design tools

In order to be able to design the devices, software by two companies are available in our group: Concept to Volume (C2V) and FEMLAB. The C2V software called Selene and Olympios is more suitable for our purposes and better known in our group. Selene Stress and Temperature software is a two-dimensional mode solver that calculates the effective refractive index of the quasi-TE and TM modes in the port waveguide. In the case of the bend solver, it calculates also the bending loss of the quasi-TE and TM of the bend modes.

The Olympios packet simulates mode propagation in the waveguide by using the two- and three-dimensional Beam Propagation Method (BPM) or two-dimensional Bi-directional Eigenmode Propagation (BEP) and can also be used for masks design. Simulations of ring resonator devices by using Olympios with BPM can only give qualitative trends because of the limitation of this method. In the two-dimensional case, the BEP method is more reliable than BPM because reflection and optical feedback can be taken into account. However, in the case of a vertical coupling configuration, BEP is not able to deal with three dimensions and does consequently not provide a realistic design, for example of coupling coefficients. Therefore a fully three-dimensional design tool is strictly necessary to obtain reliable and accurate results.

Besides the commercial tools a number of codes have been developed in this work and by others [Tan/Klunder 2002, Tan 2003 (d)]. Klunder has developed an analytical model of the response of single cylindrical microresonator in term of modal amplitudes of the straight waveguide and the microresonator modes by using scattering matrix approach for the analysis of the response obtained from the through port [Klunder 2002 (b)]. In this model several assumptions have been made: the straight waveguide is single mode, the resonator modes are propagating in one direction, the evanescent field coupling can be modeled as an abrupt process at a certain reference plane, no mode conversion and no input signal from the add port etc. This simulation model has been further worked out [Tan/ Klunder 2002] to allow the analysis of the response of single ring devices obtained at the drop port, which is more important for our project. Recently, this model has also been extended to be able to analyze the response of cascaded multiple ring devices obtained at the drop port [Tan 2003 (d)]. These simulation models can be fitted to the experimental data obtained from measurements to derive its physical parameters such as coupling coefficients, propagation loss etc.

Besides the simulation tools developed in our group, detailed analytical and numerical studies have been carried out by the Applied Analysis and Mathematical Physics (AAMP) Group, MESA⁺, University of Twente and the Institute of Radio Engineering and Electronics (IREE) who as partners of the NIAS project deal with theoretical aspects of microresonators. As a result, the AAMP was able to develop a numerical tool that calculates the coupling coefficients by using a simplified coupled mode theory [Hammer 2003]. The IREE developed a fully three-dimensional mode solver that determines the bend modes

3.1.4 Technology and facilities

Technological limitations and availability of the facilities also influence our design. The application of SiON in our group has been motivated by its excellent optical properties such as low absorption in the visible and near infrared wavelength range. Moreover, the refractive index of SiON can also easily be adjusted over a large range between 1.45 (SiO₂) to 2.0 (Si₃N₄). In addition, standard silicon substrates can be used and reliable techniques that are compatible with standard silicon integrated circuit processing are available. Conventional optical photolithography by using contact printing and standard etching processes such as wet etching and dry etching (e.g. RIE) are available in our MESA⁺ clean room. This approach opens a route for potentially low-cost mass production. Another technological issue is the minimum dimensions of structures that can be written on the mask. The Laser Mask Generator (Heidelberg Instrument DWL 2.0) that is available in the MESA⁺ clean room can manufacture masks with structures with a smallest dimension of 2 μm. On the other hand, high-resolution e-beam masks can realize structures down to 100 nm without any problems.

When we apply conventional optical photolithography with the aid of contact printing, a technique available in the MESA⁺ clean room, the use of a high-resolution e-beam mask for structures with dimension not smaller than 2 μm is not a meaningful and cost-effective option. Therefore optimizing the design to structures with smallest dimension not less than 2 μm could allow writing low-cost masks in the MESA⁺ clean room. High-resolution e-beam masks, or the application of a waferstepper with 4 or 5 times reduction, would allow producing structures with smoother surface sidewalls and consequently reduced scattering loss as the roughness on the masks will be transferred directly to the resist pattern.

3.1.5 Objectives

Another important input to the design are the objectives of the project. They are closely related to the objectives of the two projects the work in this thesis made part of. In both projects the microresonator based devices were intended for the access network and consequently should be low-cost. Besides that operation in an every-day and common environment should be possible without the need of maintenance by trained engineers. In addition the devices should demonstrate the use of microresonators as building block for VLSI photonics. For this, issues as on-chip insertion loss, waferscale reproducibility, and also the introduction of increasing complexity are of primary importance. To meet the demand on potentially low-cost fabrication our devices have been designed for high refractive index SiON/ SiO₂ or Si₃N₄/ SiO₂ in combination with available conventional technology. By using these materials and technology, the ring radius can be reduced down to 10 - 30 μm corresponding to a FSR of about 20 nm - 8 nm. This range can in some cases be extended by Vernier-type multi-ring devices allowing meaningful applications in the proposed access networks.

3.1.6 Time frame

The design activities are also limited by the time frame given by the projects and their deliverables and milestones. The two years of the BTS project allowed only for a few design iterations, as in that time the knowledge, previous experience and man-power involved was quite restricted. The still continuing NAIS project (2001-2004) could count with much better starting conditions and largely increased man-power. The milestones and deliverables, however, were much more demanding and asked for specific activities: work on multi-ring devices and build up of a characterization set-up with high spatial resolution. The number of device iterations within NAIS was high and related to deliverables. Chapter 6 and 7 reflect the most important results. Another time frame is of course the fulfillment of the academic demands of a Ph.D. thesis with an individually traceable contribution of the Ph.D. candidate in question. Especially in the NAIS project a team of 5 Ph.D. students have been or are currently involved with different overlap in time. This, of course is of great benefit for transfer of knowledge, but puts special demands on publications and reports.

3.1.7 System specifications

For the projects involved, the system specifications such as insertion loss, fiber to chip coupling loss, crosstalk etc. are of primary importance. In the BTS the system concept was still quite open, in the NAIS project, however, a specific application, a WDM transceiver module for the access network, has been chosen.

For example, the responsible partner, Nortel gives the following general requirements: a wavelength band in the range of 1530 - 1560 nm, a minimum number of 16 wavelengths, a fiber span of 10 - 20 km, a transmission speed of 1.25 Gbit/s, an optical power budget (point to point) of minimum 6 dB due to fiber loss, an optical power budget (Passive Optical Network, PON) of minimum 20 dB due to fiber loss and passive splitter (assume PON architecture with passive splitter loss of 14 dB for 16 way) and finally, a cost limit of US\$ 200 for a complete transceiver. For a bit-rate of 1.25 Gbit/s the roundtrip time should be less than a few ps. Accordingly the ring radius should not exceed 50 μm .

3.2 Field of specific activities

3.2.1 Design

After having discussed the input fields, in the following the specific activity fields will be explained in some details. In the design process first the functional performance has to be considered as given by the system specifications and objectives. Considering the requirements of the system of at least 16 wavelengths we should provide a FSR of more than 20 nm. At this moment our devices with the smallest ring radius of 15 μm have a FSR of about 14 nm, substantially lower than the expected minimum of 20 nm. However, the FSR can largely be enhanced by using a two-ring approach in a Vernier configuration [Griffel 2000 (a)].

After the first experiences with resonators in the lateral coupling configuration the vertical arrangement has been chosen because of the better controlled fabrication technology, see also Sec. 2.3.2. As the coupling coefficients in the vertical coupling configuration are determined by the phasemismatch, the thickness of the gap and the offsets in lateral direction a precise definition of the gap is essential for well working devices, see also Sec. 2.2.

A low enough phasemismatch is obtained by optimizing the effective refractive index difference of the port waveguide and the ring using available software [C2V]. In the design procedure first the effective index of the ring that allows a sufficient low bending loss is calculated. Thereafter a port waveguide with approximately the same effective index is designed with the restriction that it should be single mode at the minimum width allowed by our current lithography ($\sim 2 \mu\text{m}$). In the previous work on resonators with the vertical coupling configuration the coupling coefficients have been estimated experimentally, by fitting the simulation model to the spectral response obtained by the experiment. Our result then was that a gap of about $1 \mu\text{m}$ will give a field coupling coefficients between 0.4 – 0.6. Currently, however, the coupling coefficients can now be estimated numerically before the devices are fabricated [Hammer 2003].

The first mask design has been done for 4" mask by using Olympios software [C2V] to be able to use a complete area of a 3" wafer. A lot of ring structures have been put on the ring mask such as single ring devices with different ring radius and width, switch structures, etc. to be combined with an appropriate waveguide mask for the port waveguide. Test structures were also included like straight waveguides. Later on, due to the facilities available in MESA+ clean room, only 5" masks have been used to be able to use a complete area of a 4" wafer.

In this thesis filter devices are considered with increasingly specifically tailored performance. In the beginning single ring devices were designed with promising filter functionality. With the experiences obtained from single ring devices we designed more complex devices by cascading multiple rings in parallel arrangement. Their response show better performance than the response obtained with single ring devices such as higher ON-OFF ratio, flatter passband and lower crosstalk. Finally, spectral slicer devices based on single ring and cascaded two rings were designed and demonstrated for the first time.

3.2.2 Realization

After completing the design process, the realization step is started. As we use the vertical coupling configuration covering the port waveguides with an intermediate gap layer causes bumps on the layer stack. Even if the port waveguides are very thin a not well-defined profile of the gap layer is obtained. In order to solve this problem, Chemical Mechanical Polishing (CMP) is sometimes used for planarization. Another issue in the realization is that inspection directly after the developing of the resist layer shows that sometimes the rings can not be well aligned to the port waveguides. Consequently the photolithographic process had to be repeated. Ideally one would like to work with a mask aligner with a resolution better than 100 nanometers. Another aligning problem arises from the curvature of the wafer due to the stress after deposition of the layer stack.

Since we have a problem with the alignment of the two masks we decided to use only a small area of $2 \times 3 \text{ cm}^2$ in the center part of the mask assuming that the influence of the curvature on the wafer will probably be less for such a small area. It appears that the use of a restricted wafer area does not resolve the problem. However, some wafers consisting of several working devices have successfully been fabricated and characterized. Their results are presented in this thesis. Aligning problem due to the low resolution of the mask aligner can probably be solved by utilizing a wafer stepper with an overlay accuracy of about 100 nm or growing a layer on both sides of the wafer that might reduce the curvature effect on the wafer. Most of the devices were processed by experienced technicians of the IOMS group, first G. Sengo and L. Hilderink and later also H. Kelderman. Results from the realization step have often been used as a feedback to the design activities.

3.2.3 Intermediate characterization

Before we go to the functional characterizations of the devices, the intermediate characterization has to be done.

This step is intended for preliminary characterization of the layer thickness, refractive index, test of the lithography processes, etc. For the layer thickness and refractive index measurements, there are two methods available in our group; prism coupling and ellipsometry. The photolithographic process often had to be repeated because observation of the alignment marks before etching process shows that the rings were not well aligned with the respect to the port waveguides. In one of our samples the intermediate characterization revealed already a too thin layer. The devices, however, were completely processed and analyzed nevertheless the high roundtrip losses of the resonators (see Ch. 6).

3.2.4 Functional characterization

Functional characterization is intended to evaluate the functionality of the device. In order to be able to evaluate the device performance, two characterization set-up have been built during my PhD work, see also Sec 2.5; a standard characterization set-up for global spectral measurements that has been built and developed by using a former set-up available in our group together with another PhD student and a completely new imaging set-up for local measurements. This set-up provides precise information on the local light intensity at every part of the devices with spatial resolution down to less than 2 μm and has been built as fulfillment of a formal deliverable of workpackage 5 of the NAIS project. The performance of this set-up has largely improved after acquisition of an Infrared CCD camera that is sensitive for wavelengths around 1.5 μm (SU320M-1.7RT Indium Gallium Arsenide MiniCamera). The largely improved sensitivity (2-3 orders of magnitude) allowed higher magnification and consequently larger resolution.

In order to be able to evaluate the device performance, comparison with a simulation model has been made. This model has been made as close as possible to the real situation of the device. The device parameters were not fixed but allowed to vary freely. In this way the stability of our simulation program against small variations could be examined.

After the fitting is completed, the simulated curve should be close to the experimental spectral response and all device parameters such as coupling coefficients, propagation loss inside the ring, effective radius of bend mode, effective refractive index of the bend mode etc. can be obtained. The simulation results can also be checked by using known parameters such as the effective refractive index of the bend modes that can be calculated with Selene Stress and Temperature of C2V. This simulation processes should be iterated to obtain the best fit between the simulation model and the spectral response with reasonable fitting parameters. The result from this analysis gives an important feedback to the intermediate characterization step, the realization step and the design step where necessary improvements and modifications can be implemented.

3.2.5 System demonstrator

When the evaluations show that the device response meets the requirements, the next step is to combine all functional devices together to build a system on a single chip. The system performance should also be evaluated by comparing the results from the evaluations with the specifications that have been determined in the beginning. These evaluation results become an input for the previous steps. These steps might probably be iterated several times to achieve the expected results that meet the system requirements. When system specifications are fulfilled, therefore, we have a demonstrator device.

Conclusions

The design strategy is a complex procedure to combine previous knowledge, constraints from the system concept and availability of tools and facilities in an innovative design. The design is verified by several fabrication and characterization steps and results eventually in a demonstrator.

Design strategy

As constraints are changing and knowledge, facilities and experience continuously improving, the design strategy involves numerous feedback lines. In the course of this thesis an evolution from simple single microring to complex multi-ring devices with an improved functionality could be realized.

Chapter 4

High finesse single-ring resonator devices based on a lateral coupling configuration for WDM applications

The study of microring devices in our group has started with devices in the lateral coupling configuration. In this arrangement, both the port waveguides and the ring are located on the same layer. In order to minimize the bending loss of the ring, we need relatively high refractive index materials. The Silicon Oxynitride (SiON) technology [Wörhoff 1999, Wörhoff 2002], which is extensively used in our group, allows a broad range of refractive indices between 1.45 (SiO₂) and 2.0 (Si₃N₄) and is appropriate for this purpose. By using LPCVD Si₃N₄, the optimized dimensions of the ring are a radius of 25 μm and a width of 2.5 μm. The straight waveguide has a width of 1 μm. The thickness of both, ring and waveguide is 300 nm that is limited by the maximum thickness of Si₃N₄ layers achieved by the LPCVD process.

The standard measurement method [Tan 2003 (b)] has been used to characterize the devices. For completeness, detail on-chip measurements based on quantitative image analysis [Tan 2003 (b)] have also been done. A low on-chip insertion loss of less than 0.2 dB could be measured [Tan 2001 (b)]. The detailed experimental results of single ring devices in the lateral coupling configuration using the standard measurement method have been reported in [Tan 2001 (a)] and are presented in full in the following section.

Design of a micro-ring resonator

The layout of a microresonator is schematically given in Fig. 4.1. Light from a single-mode input channel (port 1) is coupled partly (depending on the coupling constant, κ_i) to the ring resonator, which supports several radial modes. The remaining light will propagate to the throughput port (port 2).

Light in the ring, with an effective index $n_{\text{eff},q}$ and absorption α_q , propagates half a circle and is coupled partly (with the same κ_q) to the drop port (port 4). The remaining light completes the roundtrip, couples partly back to the throughput port (port 2) - once again coupling constant κ_q - and has now a

fraction X_q of the original modal amplitude.

A second adjacent waveguide serves as an add and drop channel. For efficient coupling between the ringresonator and the input waveguide, the waveguide mode is phase-matched to the lowest order resonator mode. The coupling between the resonator and the

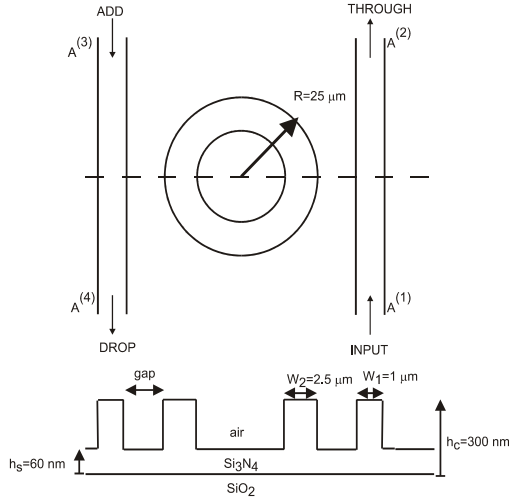


Fig. 4.1 Top-view and cross-section of the waveguide-coupled to micro-ringresonator

waveguides can be controlled by varying the gap.

Based on this model, the functional behavior of the complete device in Fig. 4.1 can be analyzed. The formal relationship between the modal amplitude at the input port $A_0^{(1)}$ and the throughput port $A_0^{(2)}$ is given by [Klunder 2000]

$$\frac{A_0^{(2)}}{A_0^{(1)}} = t_0^{(1)} - \sum_q \frac{(\kappa_q^{(1)})^2}{\mu_q^{(1)}} \left(\frac{\exp(j\rho_q)}{X_q} - 1 \right)^{-1} \quad (4.1)$$

where ρ_q is the phase shift per roundtrip in the MR and $t_0^{(1)}$ is related to the coupled fraction between straight waveguide and ring resonator modes at the input straight waveguide. The spectral response exhibits Fabry-Perot like fringes spaced by a mode-dependent free spectral range FSR_q . The FWHM value, $\Delta\lambda_q$, of the fringes is related to the finesse F_q of a certain mode (index q) by:

$$F_q = \frac{FSR}{\Delta\lambda_q} \quad (4.2)$$

In our model the normalized spectral response at the drop and throughput port of a symmetric micro-ring resonator is governed by only two parameters: the roundtrip loss (RTL) and the coupling coefficient (κ_i).

Experimental results

The devices were fabricated by LPCVD deposition of silicon nitride ($n = 1.98$) on a thermally oxidized silicon wafer [Wörhoff 1999]. Structuring was done by standard optical lithography and RIE etching. A micro-ring resonator

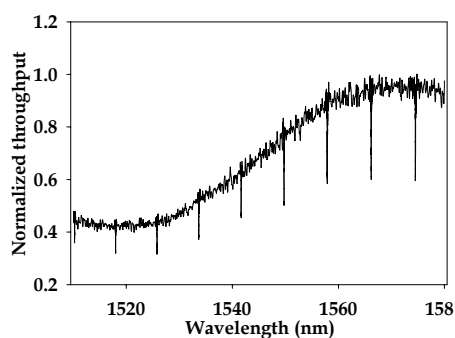


Fig. 4.2 Measured power in the throughput port of the micro-ring resonator for a gap of 750 nm

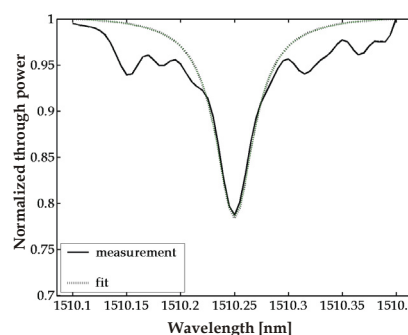


Fig. 4.3 Enlargement of Fig. 4.2 around the resonance at 1510.25 nm. Besides the experimental data also a fit by our model is given

with 750 nm gap has been characterized by launching TE polarized light of a tunable laser diode into the input port of the waveguide and measuring the power in the throughput port.

Fig. 4.3 shows the spectral response of the device in the range of 1510 to 1580 nm, which exhibits a slowly varying background level and the sharp resonance peaks separated by the FSR. The reduced transmission of the background at lower wavelengths is caused by the absorption of the SiON material itself due to the incorporation of hydrogen during the deposition process [Wörhoff 1999].

This absorption can be reduced by proper heat treatment [Wörhoff 1999]. From Fig. 4.2 the Free Spectral Range (FSR) of the fundamental ring mode can be easily determined to be 8 nm.

The higher order modes in the cavity are suppressed because of the weak coupling between the ring and the input waveguide, which can not

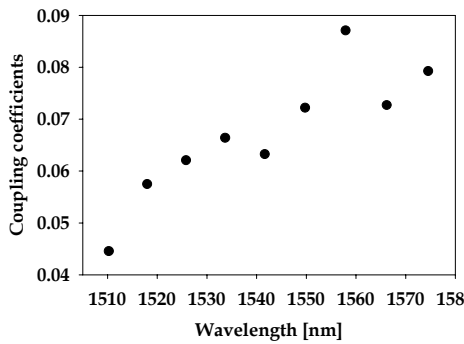


Fig. 4.4 Experimental values of the coupling coefficient obtained by the analysis of Fig. 4.2

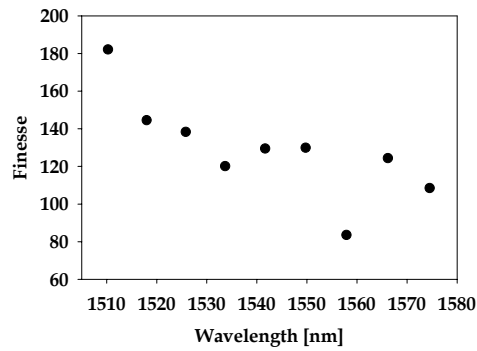


Fig. 4.5 Experimental values of the finesse obtained by the analysis of Fig. 4.2

compensate the large radiation losses. In Fig. 4.3, we give the experimental data and a fit based on our model for the resonance around 1510 nm. The analysis for this resonance with the parameters of our model results in the following experimental values: coupling constant, $\kappa_q = 4.5\%$, Finesse = 182, and FWHM = 43.92 pm (5.78 GHz). Repeating this analysis for all resonance dips we obtain Figs. 4.4 and 4.5, which show the coupling coefficients and the finesse respectively as a function of wavelength. In Fig. 4.4 an increasing coupling constant as a function of wavelength is observed as expected by the increasing overlap between the modes of the resonator and the adjacent waveguide. As a consequence the finesse will decrease as can be seen in Fig. 4.5. Once the coupling constant and the finesse are known, we can, with our model, deduce the propagation loss (α) in the cavity. This loss consists of contributions from the material itself, the scattering loss at the waveguide-air interface and the radiation loss due to bending.

The latter we can calculate numerically by a bend solver [C2V]. Subtracting the bending losses from the total losses we end up with the experimental

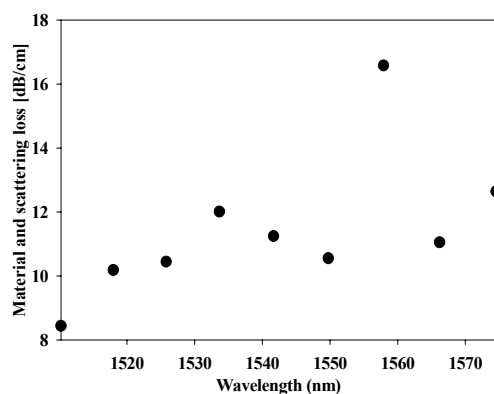


Fig. 4.6 Experimental value of the material and scattering losses in the device.

material and scattering losses as a function of wavelength, see Fig. 4.6.

Conclusions

Microring resonator devices in lateral configuration with a finesse of up to 182 and a FSR of 8 nm could be realized in $\text{Si}_3\text{N}_4/\text{SiO}_2$ technology with the aid of conventional optical photolithography.

The detailed analysis and comparison with model calculations allowed the determination of the relevant parameters like coupling coefficients and roundtrip loss. By imaging analysis an extreme small off-resonance on-chip insertion loss of less than 0.2 dB could be determined. The narrow resonance linewidth of less than 50 pm (6.25 GHz) in the wavelength range of 1510 -1580 nm is very attractive for possible dense WDM applications.

Chapter 5

Single microring resonator devices based on a vertical coupling configuration

In this chapter, single microring resonator devices with a vertical coupling configuration are discussed in detail. For the realization two alternatives have been chosen where in both cases the port waveguides were made from Si_3N_4 , the microring core, however, etched either out of a SiON or a Si_3N_4 layer, see Section 5.1 and 5.3 respectively. In the course of the work the quantitative image analysis set-up has been developed and applied for the first time to the devices described in Section 5.1. We include therefore in Section 5.2 a detailed description of these results already published in [Tan 2003 (b)].

5.1 Silicon Oxynitride based microring resonator devices

In our group the first results with microring resonators have been obtained with devices with a lateral coupling configuration, see Chapter 4. These devices were designed for TE polarization only. In this section, a feasibility study of microring resonators for telecommunication applications within the BTS project [BTS project] is presented. The proposed devices should work for TE and TM polarization.

For the realization of the devices SiON technology has been chosen as the large range of the index of refraction (1.45 - 2) provides large freedom in the design. In the design process a balance has to be found between the refractive index of the optical layers, the potential and limitations of the fabrication process and the availability of materials. In this process detailed computer simulations play a crucial role.

5.1.1 Design considerations

The devices should be potentially low-cost and consequently should be fabricated by standard clean-room technology as, for example, available in the MESA+ clean-room. The width of the waveguide should be at least $2\ \mu\text{m}$, the size limit that can be achieved by the in-house Laser Mask Generator in combination with our conventional mask-aligner.

The straight waveguides should be designed to be thin enough to avoid distortion of the above lying microring or, at least, to allow planarization of

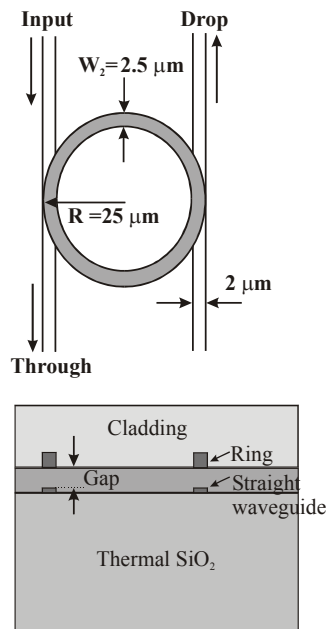


Fig. 5.1 Schematic layout (top-view) of a device in the vertical coupling configuration and its cross-section

the separation layer (see also section 2.3.2). They should, in addition, support only a single mode in vertical and horizontal direction for both TE and TM polarization. For the straight waveguide core LPCVD Si₃N₄ is chosen.

Optimization of the straight waveguide geometry with Selene Stress and Temperature [C2V] results in a straight waveguide with a width of 2 μm and a thickness of 140 nm that gives an effective refractive index of 1.509 for the fundamental TE mode and 1.469 for the fundamental TM mode.

The microring resonators have been designed to be single mode in vertical direction. In radial direction, however, higher order modes due to the geometry of the resonators can not always be neglected. These higher order modes can be suppressed by optimizing the microring resonator design. A combination of extremely low effective refractive index and consequently extremely high bending loss of the higher order modes inside the microring resonators can exclude practically all higher order modes from the spectral response of the device. This can be achieved, for example by narrowing the width of the microring waveguide.

For the application in the BTS project, the microring resonator was designed to support only a single mode in radial direction for both TE and TM polarization with acceptable bending loss. In order to fulfill these requirements, we choose PECVD SiON with a refractive index of 1.65, see also Section 2.3.2. Because of this relatively low refractive index a relatively thick layer of about 1.5 μm is needed for the ring with a 2.5 μm wide waveguide. In the following section we give the details of the fabrication process.

5.1.2 Fabrication process for the complete devices

The devices have been fabricated by means of conventional optical photolithography and Reactive Ion Etching (RIE). The waveguiding structure can not be deposited directly on 3.2 μm thick thermally oxidized wafers with a refractive index of 1.45 that are available in the MESA⁺ clean room. According to the simulation by Selene Stress and Temperature of C2V [C2V], this thickness is not sufficient to isolate the field in the waveguides completely from the silicon substrate.

Therefore, an additional PECVD SiO₂ layer with a refractive index of 1.46 (obtained with ellipsometric measurement) and a thickness of 5 μm has been

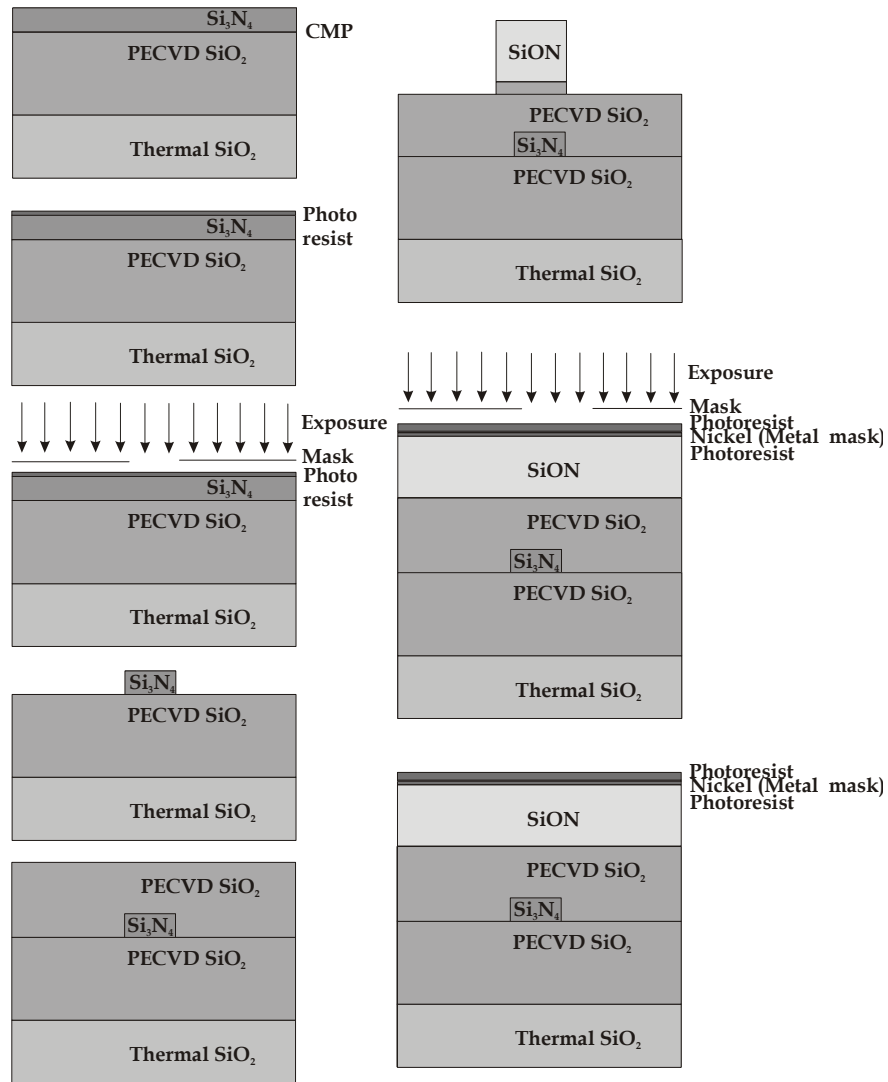


Fig.5.2 Realization of a complete device. The microring was made from PECVD SiON. The processing starts from the top left to the bottom and continues counter clockwise

deposited to extend the substrate buffer layer. This layer was deposited at 300°C. The surface roughness of the PECVD SiO₂ layer as deposited is more than 5 nm (rms).

This value was obtained with Atomic Force Microscopy (AFM) measurement for a $5 \times 5 \mu\text{m}$ surface. This surface roughness is too large when we want to deposit LPCVD Si_3N_4 on top of this layer. An annealing step would not solve this problem because the melting point of PECVD SiO_2 is relatively high and can cause stress to the layer stack. Therefore Chemical Mechanical Polishing (CMP) has been applied to remove the surface roughness of the PECVD SiO_2

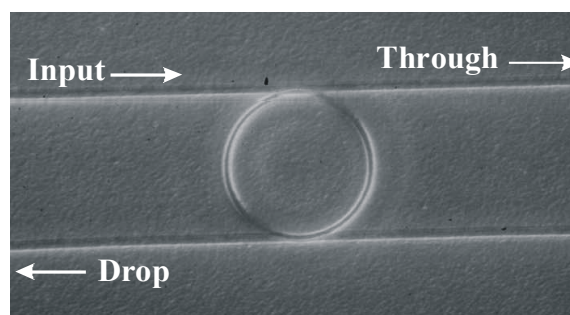


Fig. 5.3 Top-view picture of SiON based microring resonator device obtained with a 50 X microscope objective

layer. On top of this layer, a LPCVD Si_3N_4 layer of approximately 140 nm has been deposited. Conventional optical photolithography and RIE have been applied to define the straight waveguides. After that, another PECVD SiO_2 layer with a thickness of $1 \mu\text{m}$ has been deposited once again to perform a separation layer (see Fig. 5.2) between port waveguides and the ringresonator. Without any planarization process, the PECVD SiON core layer with a refractive index of 1.65 and a thickness of $1.5 \mu\text{m}$ has then been deposited. Due to the thickness of the PECVD SiON layer, we can not apply directly photolithography and RIE to pattern the microring. A standard resist layer can not withstand the long etching process and an additional mask for patterning is needed. Nickel has been chosen for this purpose because it has better properties compared to other metals such as aluminium, which is too soft for this purpose or chromium, which will crack due to the high temperature occurring during the fabrication processes [Roeloffzen 2002].

A direct contact between metal layer and ring layer should be avoided because the metal layer might not be removed completely after etching and introducing in that way additional loss. In order to minimize this possibility, on top of this layer we put photoresist with a thickness of approximately 500 nm. The photoresist is hard baked on a hot plate at 150°C for 1 hour. A nickel layer with a thickness of 150 nm is sputtered on top of the hard photoresist.

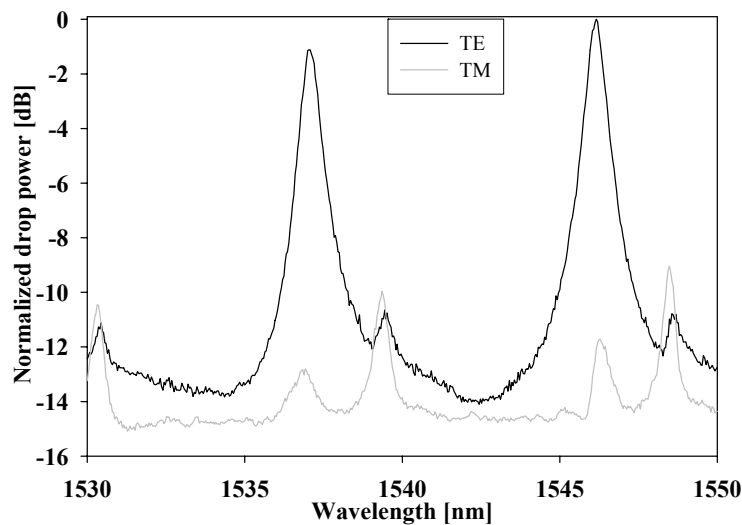


Fig. 5.4 Drop port response of a single SiON microring resonator for TE and TM polarization, normalized to the response of TE polarization

Finally, we put the second photoresist layer with a thickness of 1.3 μm for patterning. This photoresist layer has been baked at 95°C for 1 minute. Now, the photoresist is ready to be patterned. After photolithography, a post exposure bake at 120 °C for 1 minute has been applied. The photoresist is now ready to be developed. After developing (OPD 4262), Ni-etch has been applied to transfer the photoresist pattern onto the nickel layer. Finally, RIE has been used for patterning the microring resonators. After removing the photoresist the Ni-etch was applied once again to remove the nickel layer from the top of the microring resonator. A top-view microscope picture of the final devices obtained with a 50 X objective is presented in Fig. 5.3.

5.1.3 Device performance

The wafer has been cleaved to enable coupling of light to the input port of the waveguide. Characterization of the realized devices has been done for both TE as well as TM polarizations. Polarized light from a tunable laser diode has been launched and coupled to the input port of the straight waveguide by using a microscope objective (end-fire coupling). In order to have the desired polarization direction, a polarizer was put in front of the sample and behind

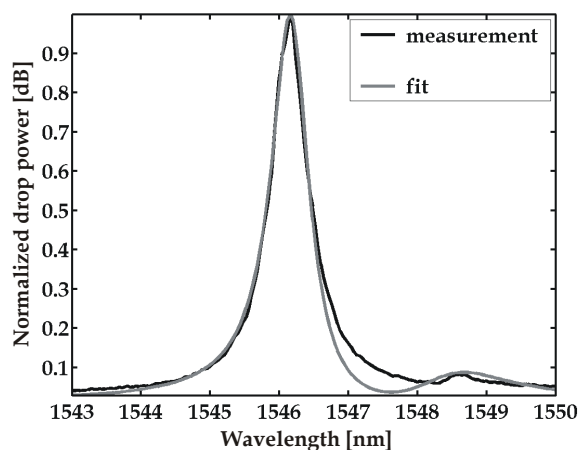


Fig. 5.5 Fitting of simulation model to the experimental data for TE polarization for a SiON microring resonator with a radius of $25 \mu\text{m}$

the sample as an analyzer. The output of the devices from the through (or drop) port is projected to a detector by using another microscope objective.

The spectral response of the device for TE and TM polarization are given in Fig. 5.4. The Free Spectral Range (FSR) is about 9.2 nm for both TE and TM polarization. A finesse of about 14 (FWHM ~ 0.6 nm) for the fundamental TE mode and about 19 (FWHM ~ 0.48 nm) for the fundamental TM mode could be observed. No polarization conversion could be observed in this experiment by changing the polarization direction of the polarizer and the analyzer.

The calculated bending loss of this device obtained by Selene Stress and Temperature [C2V] is about 0.67 dB/cm for the fundamental TE mode and about 0.82 dB/cm for the fundamental TM mode.

Fig. 5.4 shows not only the fundamental modes of TE and TM polarization but also the first order radial mode. These higher order modes are present in the spectral response because the bending loss of the first order radial mode

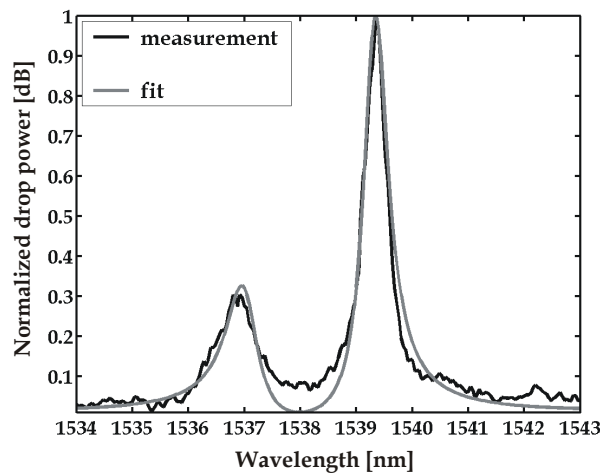


Fig. 5.6 Fitting of simulation model to the experimental data for TM polarization of the SiON microring resonator with a radius of 25 μm

are not extremely high (88 and 55 dB/cm for the first order radial TE and TM mode respectively, corresponding to 1.4 and 0.9 dB per roundtrip). Their effective refractive index, however, are already below the refractive index of the background.

In order to be able to analyze the device responses, a simulation model has been developed [Tan/Klunder 2002] by using a previous model available in our group [Klunder 2002 (b)]. In this model, the coupling coefficients on both sides are assumed to be equal. Fig. 5.5 shows an example the fitting result of the device response around the resonant wavelength at 1546 nm for TE polarization by taking only part of the spectral response that represents the fundamental and the first order radial modes. Only a single resonance is given as the spectral response has periodic properties.

By fitting the simulation model to the experimental data, the propagation loss of the fundamental mode was estimated to be 73 dB/cm and the first order radial mode is estimated around 258 dB/cm, both for TE polarization. The high propagation loss of fundamental mode is probably due to the metal mask that could not be removed completely after etching. The coupling coefficient was estimated about 0.24 for the fundamental and 0.19 for the first order radial

Parameters	TE ₀	TE ₁	TM ₀	TM ₁	Method
Effective refractive index	1.511	1.419	1.509	1.424	Calculation
Bending loss (dB/cm)	0.6	86	0.8	54	Calculation
Propagation loss (dB/cm)	73	258	44	82	Fit of model to experiment
Coupling coefficient	0.24	0.19	0.26	0.22	Fit of model to experiment
FSR (nm)	9.2	9.2	9.2	9.2	Measurement
FWHM (nm)	0.6	1.5	0.48	0.6	Measurement

Table 5.1 Summary of parameters of the fundamental and the first order radial TE and TM bend modes

mode. We can apply the same procedures for the case of TM polarization. The fitting result is presented in Fig. 5.6 where the propagation loss of the fundamental mode was estimated to be 44 dB/cm and the first order radial mode is estimated of about 82 dB/cm. The coupling coefficient is 0.26 for the fundamental and 0.22 for the first order radial mode. A summary of the parameters of the fundamental and the first order radial modes are given in Table 5.1. The resonant wavelengths shown in Fig 5.4 are different for TE and TM polarization due to the difference between the effective refractive index of the TE and TM mode. The resonant wavelength shift due to the effective refractive index difference $\Delta N_{effTM-TE}$ is given (in term of frequency) by [Roeloffzen 2002]

$$\Delta f_c = \frac{\Delta N_{effTM-TE}}{N_{eff}} f_c \quad (5.1)$$

where N_{eff} is the effective refractive index and f_c is the resonant frequency. By inspecting Eq. (5.1), the resonant wavelengths shift of the TE and TM polarization can be estimated. Inserting the effective refractive index difference of the fundamental TE and TM mode given in Table 5.1 one expects a shift of 2 nm as also observed experimentally (see Fig. 5.4).

These measurements show that it is difficult to use single-ring resonator devices based on SiON technology for making polarization independent wavelength filters. A possible solution is described by Klunder et al. [Klunder 2002 (a)] who propose a polarization diversity scheme together with cascading of several rings.

In order to complete the information of the device, a detail on-chip characterization based on quantitative image analysis has been done. This characterization method and its results have been reported in [Tan 2003 (b)] and are reproduced in the following section.

5.2 Characterization of vertically waveguide coupled microring resonators by means of quantitative image analysis

In our group, high Finesse microring resonators have been fabricated and demonstrated [Klunder 2001, Tan 2001 (a)]. They are fabricated based on SiON technology [Wörhoff 1999] and are laterally coupled to input and output waveguides. This configuration can be realized relative easily in a one-step lithographic process. In this way the ring resonator and the straight waveguides are structured out of the same layer stack. A drawback of this method, however, is that the resonator and waveguides can not be optimized independently. Moreover this configuration is relatively sensitive to the variations of the definition of the gap between the ring resonator and the adjacent waveguides and therefore requires a very rigorously controlled photolithographic step.

In order to overcome this problem a vertically waveguide coupled microring resonator is proposed [Klunder 2001].

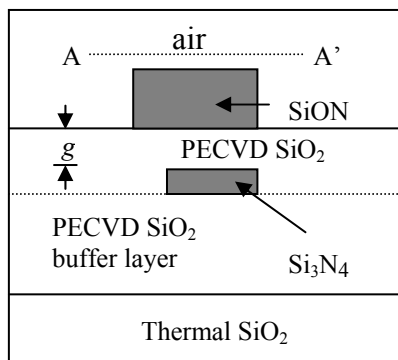


Fig. 5.7 Schematic cross-section of the vertically coupled waveguide-microring resonator taken at line A-A' in Fig. 5.8

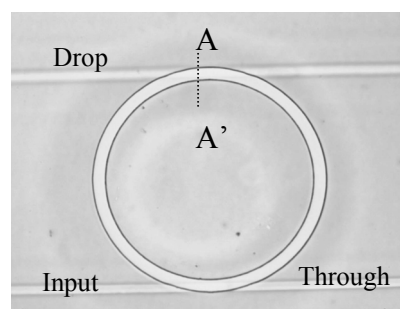


Fig. 5.8 Photograph of a device with the ring resonator structure visible in the developed resist layer with radius of $25 \mu\text{m}$

This configuration is more tolerant to the variations of the technology, especially with respect to the gap definition as the thickness of the separation layer between the MR and the underlying straight waveguides can be well controlled.

	Ring resonator		Straight waveguide 0 th order
	0 th order	1 st order (leaky modes)	
$N_{eff, TE}$	1.511	1.419	1.509
$N_{eff, TM}$	1.509	1.424	1.469
$\alpha_{bend, TE}$ (dB/cm)	0.6	86	-
$\alpha_{bend, TM}$ (dB/cm)	0.8	54	-

Table 5.2 Summary of the simulation results for TE and TM modes

For its realization, however, at least a second photolithographic step is needed. Therefore alignment of the masks becomes a critical issue.

For the characterization of the devices, normally the standard method is used whereby the global response of the device is determined by measuring the output (through or drop) ports as a function of incoming wavelength. Additional local information, however, such as on-chip insertion loss, on-chip drop efficiency etc. becomes important when cascading of the ring resonators is considered in the case of complex photonic circuits. This information can be obtained by applying quantitative image analysis as a complementary method. In the following we demonstrate the reliability of the quantitative image analysis method by comparing their results with measurement results obtained by the global standard method.

Vertically Coupled Microring Resonators

The devices have been fabricated based in SiON technology [Wörhoff 1999] in combination with conventional optical lithography and Reactive Ion

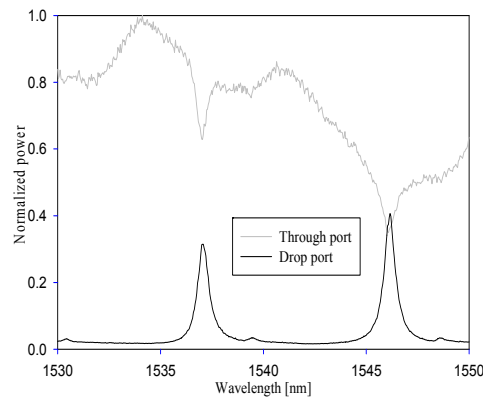


Fig. 5.9 Spectral response of the MR with radius 25 μm for TE polarization

Etching (RIE). A cross-section of the vertical coupling device is given in Fig. 5.7 and a top view photograph of a realized device with a separation layer of 1 μm in Fig. 5.8.

The waveguides are embedded in Plasma Enhanced Chemical Vapor Deposition (PECVD) SiO₂ and function as input and output port.

In order to minimize the bump in the separation layer which is caused by the straight waveguides underneath, a relatively thin core layer has been designed. By using high refractive index ($n = 1.98$) Low Pressure Chemical Vapor Deposition (LPCVD) Si_3N_4 [Wörhoff 1999] as core material, the core thickness of the single mode waveguides with a width of $2 \mu\text{m}$ could be reduced to $0.14 \mu\text{m}$.

The ring resonator on top of the layer structure is made of PECVD SiON ($n = 1.65$) that has been etched deep to achieve sufficient contrast and acceptable bending loss. The ring sustains only a single mode in vertical direction. In radial direction the higher order modes have much higher bending loss than the fundamental mode and can be suppressed by an appropriate design. The

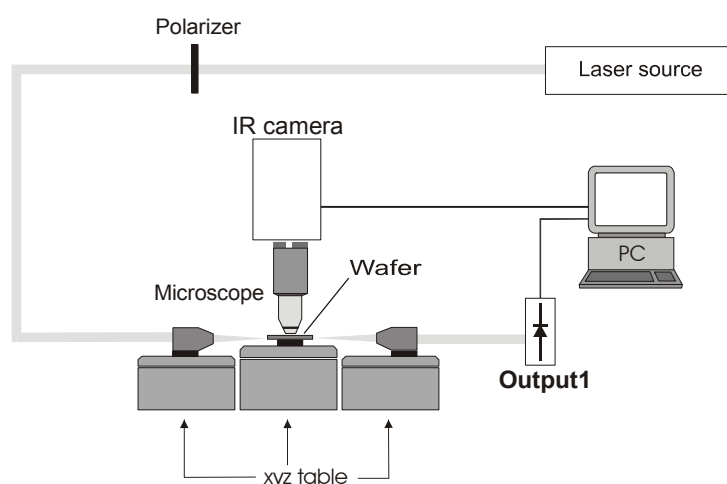


Fig. 5.10 A schematic layout of the experimental set-up used for collecting the scattered light from the top of the device

dimensions of the ring resonator are as follows: radius $25 \mu\text{m}$, thickness $1.5 \mu\text{m}$ and width $2.5 \mu\text{m}$. The straight waveguide and the ring resonator have been designed carefully to have only a small phase mismatch between each others, low propagation loss and sufficient coupling. During the fabrication process Chemical Mechanical Polishing (CMP) has been applied to remove the surface roughness of the PECVD SiO_2 buffer layer. A summary of the simulation results of this device is given in Table 5.2.

The device has been characterized for both TE and TM polarization by using the standard characterization method. Fig. 5.9 shows the spectral response of the device as a function of wavelength for TE polarization. An analysis of the curves results in: FSR ~ 9 nm, FWHM ~ 0.6 nm and Finesse ~ 15 .

In order to test the reliability of the quantitative image analysis method we have only considered the case of TE polarization. However, the same procedure can also be applied to the case of TM polarization.

Experimental set-up

In order to characterize the device, we launched TE polarized light from a tunable laser diode at wavelengths around 1550 nm with the aid of a

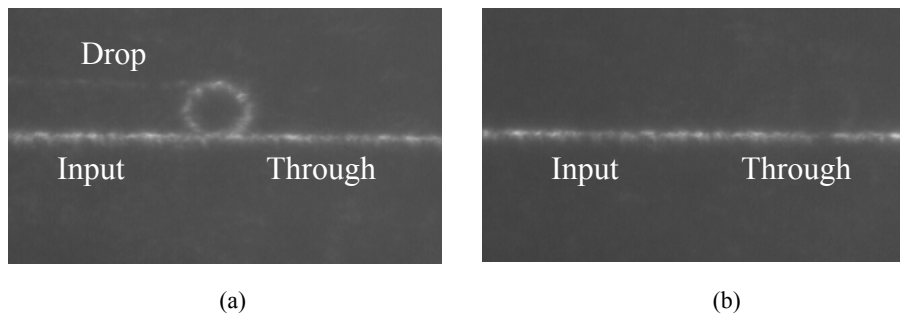


Fig. 5.11 Images obtained by the IR camera of a MR; (a): on-resonance, (b): off-resonance

microscope objective (end-fire coupling). For the standard measurements, the output of the device was collected by another microscope objective at the backside of the device and projected on a detector (HP 81521B). In the case of the quantitative image analysis, the scattered power from the device has been projected by a lens system to the IR vidicon camera (Micronviewer model 7290*), Electrophysics) to produce the image. After image processing and correcting for the nonlinearity of the camera response, the quantitative spectral response curves were obtained.

*) presently a CCD camera with enhanced performance is available

Fig. 5.10 shows a schematic layout of the experimental set-up that was used to characterize the device.

Quantitative image analysis

A high NA reflecting microscope objective has been used to collect the scattered light of the device and projected it to the IR camera. Fig. 5.11a shows

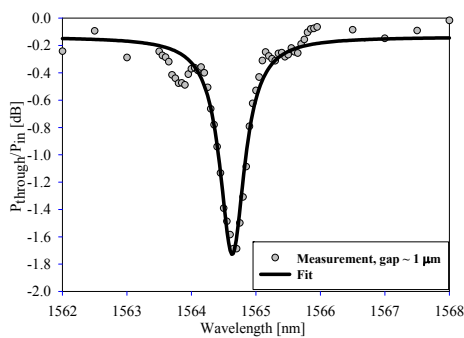


Fig. 5.12 The through port power of a MR around 1564.65 nm obtained by quantitative image analysis

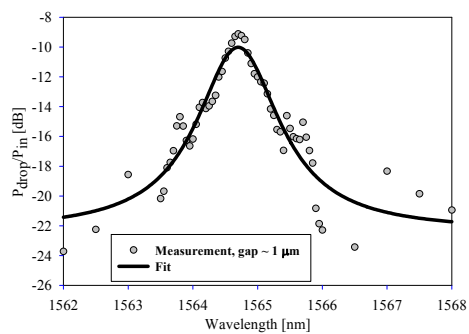


Fig. 5.13 The drop port power of a MR around 1564.65 nm obtained by quantitative image analysis

the MR with the wavelength set on-resonance resulting in high intensity inside the MR and partly coupling of light to the drop port. Fig. 5.11b shows the off-resonance picture where most of the power remains in the straight waveguide and is transferred to the through port. By scanning the wavelength of the tunable laser, the IR camera registers the response of the MR as a function of wavelength. Image processing software was used to determine quantitatively the intensities locally at the through and drop port resulting eventually in plots of the response as a function of wavelength. Fig. 5.12 and Fig. 5.13 show the through power and the drop power respectively as a function of wavelength obtained from the quantitative image analysis. For comparison, measurements around the same resonance wavelength have been performed by the standard global measurement method as shown in Fig. 5.14 and Fig. 5.15.

Both methods show a dip of the through power with the same depth of approximately 1.65 dB as described in Fig. 5.12 and Fig. 5.14. For the drop

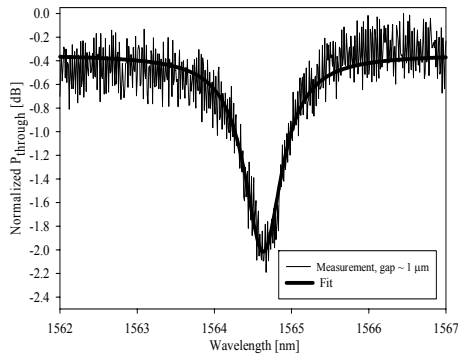


Fig. 5.14 Through port power of the MR around 1564.65 nm obtained by the standard measurement

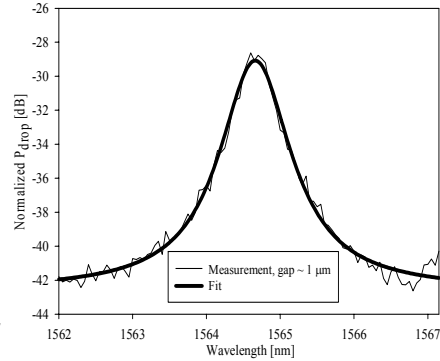


Fig. 5.15 Drop port power of the MR around 1564.65 nm obtained by the standard measurement

port, Fig. 5.13 and Fig. 5.15 show almost the same maximum of drop power around 13 dB. By comparing these results, one can conclude that this method is reliable for obtaining detailed information of the device.

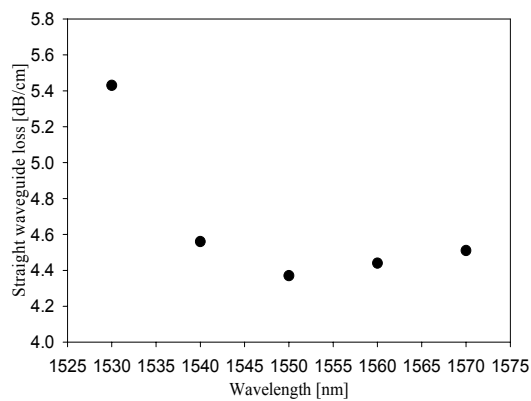


Fig. 5.16 Straight waveguide loss as a function of wavelength

The quantitative image analysis is also able to provide other local information like the loss of the straight waveguide as a function of wavelength as demonstrated in Fig. 5.16.

The loss was 4.5 dB/cm around the resonance at 1564.65 nm. The enhanced loss around 1530 nm is due to N-H overtone vibration, observed typically for as deposited PECVD SiON [Hussein 2001]. In addition, by making use of Fig. 5.12 and the propagation loss in the straight waveguide we can determine the on-chip insertion loss of the device at off-resonance to be less than 0.1 dB. Analysis of the power in the drop port results in an on-chip drop efficiency, ($P_{\text{drop}}/P_{\text{in}}$) of about 10 %.

5.3 Silicon Nitride based microring resonator devices

In the foregoing we described in detail the design, fabrication and characterization of SiON based single microresonators in the vertical coupling arrangement. In this section, the potential of Si₃N₄ based ring resonators is studied as part of a complex configuration foreseen within the NAIS project. In the following we give results obtained with single microring devices. In Ch. 6 we present our results with more complex devices based on multiple microrings.

The devices described in the following make use of LPCVD Si₃N₄ for the core of the straight waveguide as well as of the microring resonators. The effective refractive index difference between the straight waveguides and the microring resonators again has been optimized to be as low as possible to have a sufficiently low phasemismatch as discussed previously.

5.3.1 Design considerations

For the application in the NAIS project, the straight waveguide is designed to support only a single TE mode in vertical and horizontal direction. It appears that the design described in Sec. 5.1.1 is a good choice also for the present case.

The microring resonator has been designed to work only for TE polarization. Applying similar considerations as given in Sec. 5.1.1 we end up with a ring resonator with a radius of 25 μm, a width of 2.5 μm and a thickness of 300 nm. The details of the fabrication process for complete devices are given in the following section.

5.3.2 Fabrication process for the complete devices

The fabrication process of the complete devices is up to the separation layer between port waveguides and ringresonator identical to the scheme presented

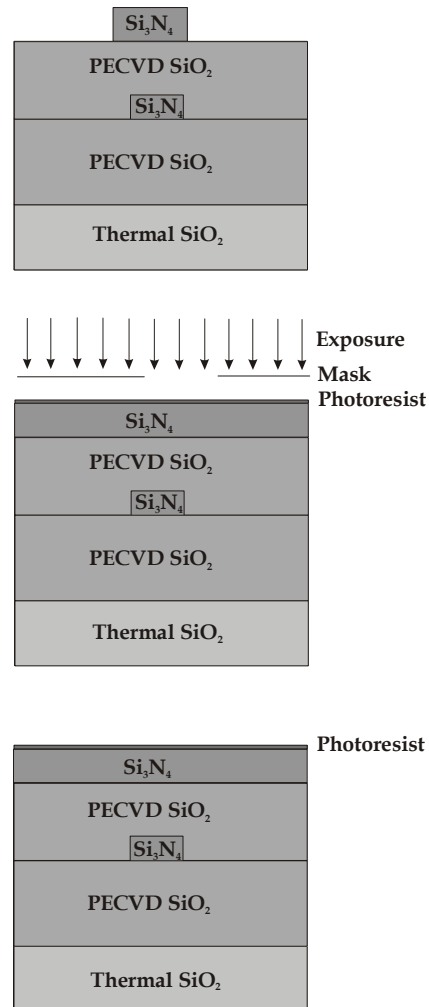


Fig. 5.17 Realization of a complete device based on a Si_3N_4 core for the port as well as the ring waveguide. Only the last three steps starting from the deposition of the ring layer are given as the previous steps are identical to the left column of Fig. 5.2. The processing starts from the bottom to the top

in Sec. 5.1.2 and Fig. 5.2. The separation layer is only made slightly thicker ($1.3 \mu\text{m}$ instead of $1 \mu\text{m}$).

On top of this layer a LPCVD Si_3N_4 layer was deposited with a thickness of 300 nm that supports only the TE fundamental resonator mode in radial direction with an acceptable bending loss. Conventional optical photolithography and RIE are applied to pattern the microring resonator. Details of the fabrication procedures are shown in Fig. 5.17. A top-view of a device obtained with a 50 X microscope objective is presented in Fig. 5.18.

5.3.3 Device performances

The devices have been characterized by means of the standard measurement method [Tan 2003 (b)]. A FSR of about 8 nm and a finesse of more than 100

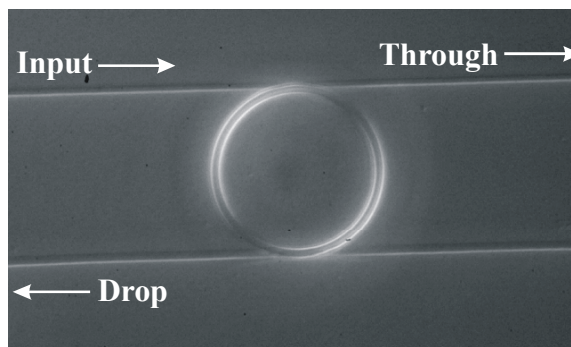


Fig.5.18. Top-view of a single Si_3N_4 microring resonator device with 25 μm ring radius obtained with a 50 X microscope objective

could be measured. The high finesse is mainly due to low loss in the ring and the weak coupling. The devices, however, show also first order radial modes with the same FSR but a substantially lower finesse of only 4. The propagation loss of the fundamental microring resonator mode is estimated to be about 14 dB/cm corresponding to 0.22 dB/roundtrip.

The functionality of this device has also been tested by launching TM polarized light. There is no detectable response from the microring resonator as expected for a device designed only for TE polarization. More details have been reported in [Tan 2002 (a)] that is reprinted in the following section.

5.3.4 High finesse vertically coupled waveguide-microring resonators based on Si_3N_4 - SiO_2 technology

Design and fabrication of microresonator devices

The fabrication of our devices is based on Si_3N_4 - SiO_2 technology [Wörhoff 1999] in combination with conventional optical lithography and RIE. A schematic layout of the device is given in Fig. 5.19 and a realized device in Fig. 5.20, where vertical coupling between waveguide and ring has been used. In

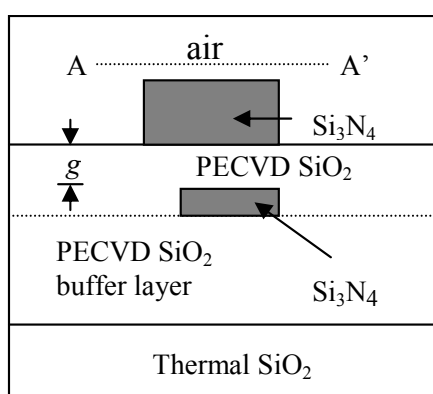


Figure 5.19 Cross-section of the vertically coupled waveguide-microring resonator taken at line A-A' in Fig. 5.20

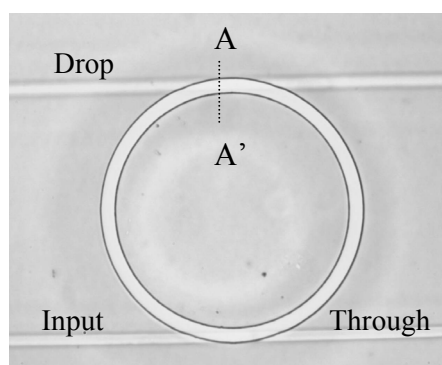


Figure 5.20 Photograph (magnification 100 X) of a device with resist on top of the ring resonator with radius $25\ \mu\text{m}$

this way the different waveguiding layers can separately be optimised in contrast to a lateral coupling structure. By using the appropriate refractive index a sufficiently large mode profile of the straight waveguide can be obtained for optimized fiber to chip coupling while single mode waveguiding is maintained. The vertical coupling structure can reduce the difficulty of the definition of the gap that controls the coupling between ring and waveguides, because the gap is defined by the thickness g of the separation layer (see Fig. 5.19). This thickness can be easily controlled during the deposition process.

Therefore the vertical coupling structure is expected to be more tolerant to variations of the technological parameters than the lateral coupling structure where the gap should be defined by critical submicron photolithography.

In order to minimize fiber to chip coupling problems and to reduce the optimal thickness of the overgrowing separation layer high refractive index Low Pressure Chemical Vapor Deposition (LPCVD) Si_3N_4 has been chosen as core materials of the straight waveguides. These waveguides are embedded between a Plasma Enhanced Chemical Vapor Deposition (PECVD) SiO_2 buffer layer and a PECVD SiO_2 separation layer. The cross section of the straight waveguide is relatively small, only $2 \mu\text{m} \times 0.14 \mu\text{m}$ to maintain single mode characteristics.

The ring on the top of the layer structure with an air cladding sustains only a

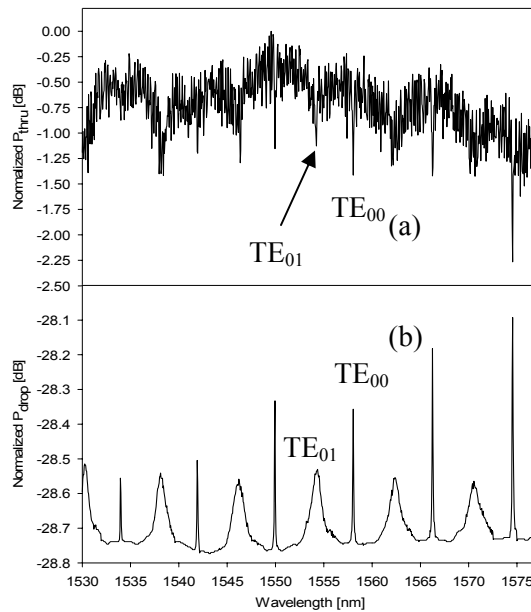


Figure 5.21 Through (a) and drop responses (b) of a microring resonator with radius $25 \mu\text{m}$ and gap $1.3 \mu\text{m}$

zero order mode in vertical direction while higher order modes are allowed in radial direction. The higher radial order modes, however, have higher bend losses and can be suppressed by an appropriate design. The dimensions used for the ring resonator are: radius $25 \mu\text{m}$, thickness $0.3 \mu\text{m}$ and width $2.5 \mu\text{m}$.

The straight waveguide and the ring resonator have been designed carefully to meet the demands on small phase mismatch between each

other, low propagation loss and sufficient coupling as mentioned in [Klunder 2001].

During the fabrication process Chemical Mechanical Polishing (CMP) has been applied to remove the surface roughness of the PECVD SiO₂ buffer layer and planarization of the PECVD SiO₂ separation layer. As an example we show in Fig. 5.20 the photograph of one of our devices with a separation layer of 1.3 μm. The effective index of this ring for the fundamental TE mode $n_{eff} \sim 1.53$ results in a calculated bend loss of circa 2.5 dB/cm; for the straight waveguide one has $n_{eff} \sim 1.51$.

Results and discussions

In order to characterize the device, we launched TE polarized light of a tunable laser diode to the input port of the straight waveguide and measured the spectral response in the 1550 nm region. Fig. 5.21 shows the responses of the devices at the 'Through' (Fig. 5.21a) and 'Drop' (Fig. 5.21b) ports.

Analysis of the spectral response by using a detailed fitting procedure as described in [Klunder 2000], gives for the fundamental TE₀₀ mode: Free Spectral Range (FSR): 8 nm, Finesse: 118 and propagation loss about 14 dB/cm for a wavelength around 1533 nm. This loss is mainly attributed to the surface roughness of the ring resonator. In addition we observe also the first order radial TE₀₁ mode, which has nearly the same FSR of 8 nm but much lower Finesse (~ 4) due to high bend losses. Fig. 5.21 shows also more pronounced dips (or peaks) of the fundamental mode for increasing wavelengths. This indicates strong coupling, which is in agreement with the results of our fitting procedure. Stronger coupling, however, due to higher field overlap results in a decreasing Finesse.

Our resonators have been optimised for TE polarization, as it is difficult or even impossible in practise to obtain polarization independent behaviour. Only a careful design with simultaneous wavelength trimming [Chu 1999 (a)] could avoid this drawback. Another approach is to employ a polarization-diversity scheme [Klunder 2002 (a)].

Conclusions

Microring resonator devices with the vertical coupling configuration have been realized by conventional optical photolithography in SiON and Si₃N₄ technology for two different WDM applications.

Moderate high index SiON ($n = 1.65$) has been chosen as core for the microring within the BTS project in order to obtain polarization independent wavelength filters. It appears that it is difficult to obtain with single ring structures polarization insensitive wavelength filters.

As in the NAIS project a polarization diversity scheme is considered, the resonator devices can be optimized for a single polarization (TE). Therefore high index Si₃N₄ has been chosen as core material. Microrings with a finesse of more than 100 have been realized and demonstrated. Also in the case of vertical coupling the high finesse is due to the weak coupling between the port and ring waveguides and the relatively low propagation loss of the resonators.

Chapter 6

Cascaded multiple microring resonators as optical bandpass filters

In the previous chapters, devices consisting of single microring resonators have been discussed. A lot of effort has been put to gain a deep understanding of the filter characteristics of the device response and minimizing the misalignment between the straight waveguides and the microring resonators in vertical coupling configuration.

Devices consisting of only single microring resonators have already been shown to exhibit a promising functionality as optical filter. The ON-OFF ratio of the device response can mainly be tuned via the coupling coefficient, κ and the propagation loss, α [Tan 2003 (c)]. The value of κ is determined by the thickness of the gap layer, the phasemismatch and the offsets in lateral direction. The major contributions to the propagation loss, α_{prop} are the radiation loss due to bending, α_{rad} , the absorption loss, α_{abs} and the scattering loss, α_{scat} :

$$\alpha_{prop} = \alpha_{rad} + \alpha_{abs} + \alpha_{scat} \quad (6.1)$$

A low bending loss can be achieved by using an appropriate geometry of the microring resonators and a high enough refractive index of the resonator core. The material loss, which is mainly due to absorption can be minimized by a special treatment, in the case of SiON by applying an anneal step [Hussein 2001, Wörhoff 1996, Wörhoff 1999]. The scattering loss originates mainly from surface roughness of the interfaces with high index contrast and can be reduced by an improved lithography and etch technology and by smoothing the sidewalls [Ladouceur 1994].

Even after optimizing the filter characteristics and improving the resonator losses, single resonator devices do not fulfill all expectations as the Lorentzian shape of the filter response does not provide sufficient freedom to synthesize the desired filter response. For a single ring device only a relatively low ON-OFF ratio, lack of the passband flatness and a narrow stopband rejection [Tan 2003 (e), Yanagase 2002] can be obtained.

Higher order filters based on cascading multiple microring resonators offer a substantial improvement of the device performance [Chu 1999 (d), Griffel 2000, Grover 2002, Kokubun 2002, Little 2000 (b), Ma 2001, Madsen 1999, Melloni 2001, Orta 1995, Tan 2003 (e), Yanagase 2002]. Cascading multiple microring resonators results in additional design freedom so that a box-like response can be synthesized with broad and flat stop- or passband, large ON-OFF ratio and sharp roll-off (defined by $\Delta\lambda_{10\text{dB}}/\Delta\lambda_{3\text{dB}}$).

The higher order filters can be arranged in serial or parallel configurations. In this chapter, however, only higher order filter in a parallel configuration will be discussed in detail.

6.1 Design of cascaded multiple microring resonators in the parallel configuration

Like in the case of single resonator devices described in Ch. 5 we designed single mode port waveguides for TE polarization with a width of 2 μm and a thickness of 140 nm to be made of LPCVD Si_3N_4 . The microring resonators are also made from LPCVD Si_3N_4 and have been designed to be single mode in vertical direction for TE polarization. Also for the radial direction single mode behavior could be obtained by reducing the width to 2 μm . The radius of the microring is 25 μm and the thickness is 300 nm. As discussed before, the phasemismatch between the straight waveguide and the microring resonator has been minimized to allow efficient coupling between port waveguides and ring. In the following the fabrication process is given in some detail.

6.2 Fabrication process of cascaded multiple microring resonators in the parallel configuration

In principle, the fabrication processes for the devices are quite similar to the

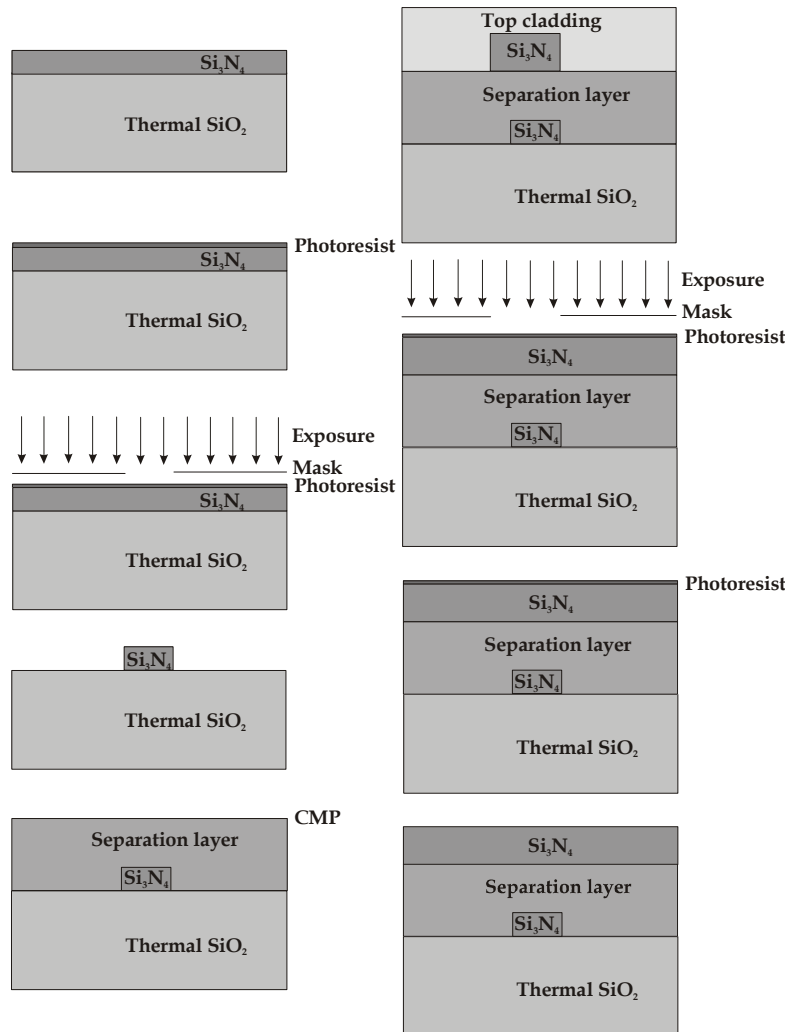


Fig. 6.1 Realization of a multi-ring device. The straight waveguides and the microrings are made of Si₃N₄. The separation layer is either TEOS or PECVD SiO₂. The top cladding is Spin on Glass or air. The processes start at the top left and continue counter clockwise

fabrication of single Si₃N₄ ring resonators.

The fabrication steps are presented in Fig. 6.1. They are based on conventional optical photolithography and RIE or Deep RIE.

The devices have been built on thermally oxidized wafer with a thickness of 8 μm . On top of this layer, a LPCVD Si_3N_4 layer of approximately 140 nm has been deposited. Conventional optical photolithography and Deep RIE has been applied to define the straight waveguides.

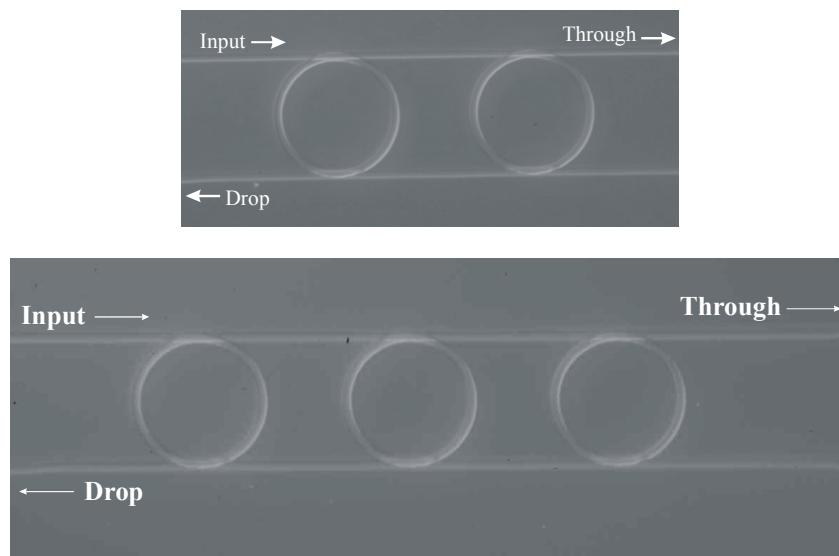


Fig.6.2. Top-view of the realized cascaded multi-ring devices with a ring radius of 25 μm obtained with a 50 X microscope objective. Top picture: two-ring device; bottom picture: three-ring device.

For the two-ring devices, we deposited Tetraethylorthosilicate (TEOS) oxide with a refractive index of 1.427 and a thickness of 1 μm as separation layer. Without previous planarization, we deposited LPCVD Si_3N_4 with a thickness of 200 nm (due to a processing error, according to the design it should be 300 nm) as a microring resonator core. Conventional optical photolithography and RIE have been used for patterning. On top of this layer we deposit Spin on Glass (SOG) with a refractive index of 1.379 as a top cladding to reduce the surface scattering loss.

For the three-ring devices, the separation layer consists of PECVD SiO₂ with a refractive index of 1.46 and a thickness of 1 μm. After deposition, planarization was done by CMP. A 300 nm thick LPCVD Si₃N₄ layer has then been deposited as the microring core layer. Conventional optical photolithography and RIE have been used for patterning the resonator. No top cladding layer has been applied. In order to reduce the losses, the device has been annealed at 1150°C for 4 hours to reduce the hydrogen content [Hussein 2001, Wörhoff 1996, Wörhoff 1999]. Top-view pictures of the final two- and three-ring devices obtained with a 50 X microscope objective are given in Fig. 6.2.

6.3 Simulation model of cascaded multiple microring resonators in the parallel configuration

For the design of the multi-ring devices and the analysis of the experimental wavelength response, a simulation model of cascaded multiple microring resonators in the parallel configuration has been developed. The basic layout of the devices together with the relevant model parameters are given in Fig. 6.3.

Light is fed into the input port of the straight waveguide and couples in part to each of the resonators. Each coupler is described by a two-parameters approach, the coupling coefficient, κ_m^n and the coupling loss, χ_m^n , where m represents the m^{th} ring and n (1 or 2 for the coupling to the input or drop port respectively) is related to the coupler position. It is assumed that light propagates in a unique direction as shown in Fig. 6.3 and that there is no direct interaction between neighboring rings. The field amplitudes in the straight waveguide and the microring resonator at each reference plane are given by a_m^n and c_m^n respectively. Additional parameters in the model (see also Fig. 6.3) are the propagation loss inside the ring, α_m , the phase shift, ϕ_m , the radius of the ring, R_m and the distance of center to center between two microring resonators, L .

For the analysis, reference plane 1 (S_1) has been used as a global reference. On the basis of this model parallel cascaded two- and three- ring resonators have been developed. In order to be able to analyze the experimental results, the model has been transferred into a Matlab program [Tan 2003 (d)]. The analysis

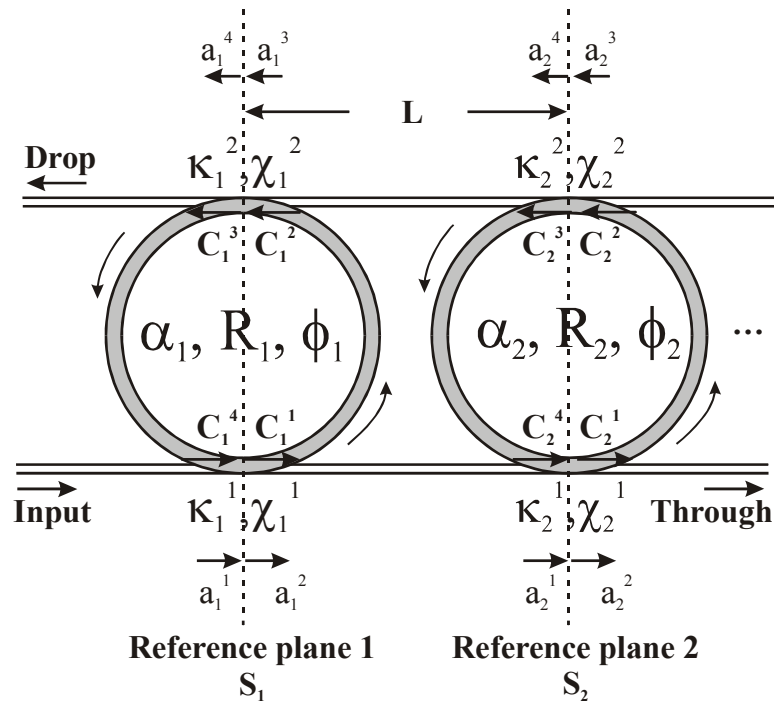


Fig. 6.3 Basic lay-out of cascaded multiple microring resonators in the parallel configuration with the parameters used in the analysis

has been performed by fitting the model to the experimental data in order to obtain important physical parameters of the device such as the propagation loss inside the microring resonator, coupling coefficients, effective radius of the microring resonator mode, etc.

6.4 Experimental results

The spectral response measurements have been done by means of the standard measurement method [Tan 2003 (b)].

TE polarized light was launched to the input port (see Fig. 6.2) of the straight waveguide by using a microscope objective lens (end-fire coupling). The

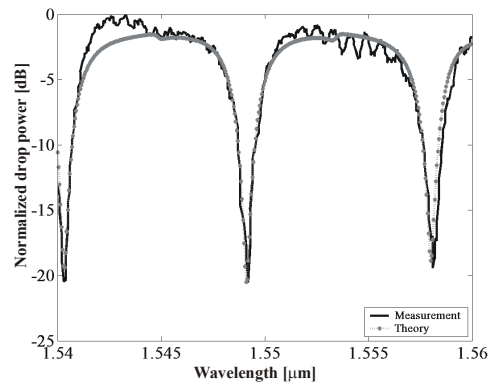


Fig. 6.4 Drop response of cascaded two-ring resonators as a function of wavelengths with equal coupling coefficient for both rings; experimental data: solid black line; simulation with fitted parameters: gray dotted line

output of the drop port was collected by another objective lens and was projected to a detector.

A first set of devices has been characterized and analyzed. During

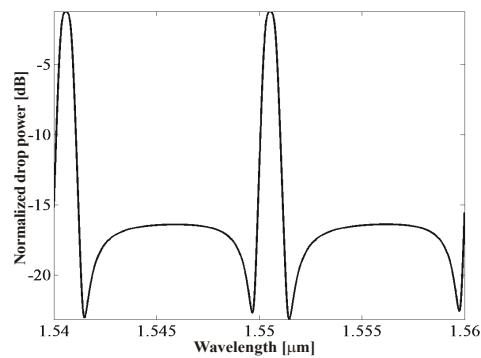


Fig. 6.5 Simulation of the drop response of a cascaded two-ring resonator with an individually optimized coupling coefficient for each of the rings

fabrication an error has been made in the thickness of the two-ring core layer (200 nm instead of 300 nm) as mentioned previously resulting in extremely high losses in the microrings.

The devices nevertheless have been analyzed as they allow still a proof of principles and verification of the model. The filter response obtained from the drop port and a fit by the simulation model is presented in Fig. 6.4. The filter response shows an ON-OFF ratio of 20 dB, which is in agreement with the prediction of the simulation model. By fitting the simulation model to the experimental data, the propagation loss of the microring resonator has been determined to be 130 dB/cm or 2 dB/roundtrip. This loss is mainly dominated by 120 dB/cm bending loss due to the above mentioned fabrication error. It can be suppressed down to 3.5 dB/cm by increasing the ring thickness, t_{ring} to 300 nm (as it was done in the three-ring devices).

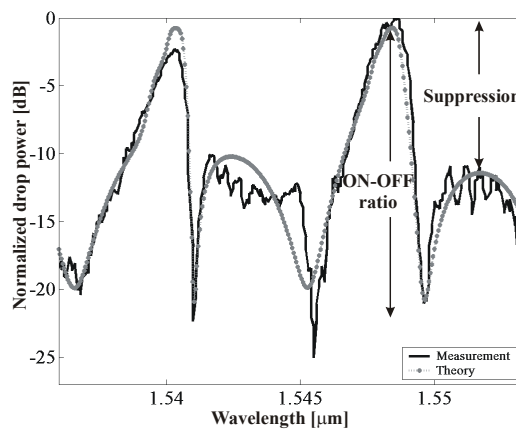


Fig. 6.6 Drop response of cascaded three microring resonators as a function of wavelengths with equal coupling coefficient for all rings; experimental data: solid black line; simulation with fitted parameters: gray dotted line

Apart from the high losses, this result shows promising filter characteristics as a bandpass filter. Unfortunately, the bandwidth of the passband is relatively wide and the rejection band becomes narrow. It is due to the strong and equal coupling coefficients of both microring resonators being 0.87. Strong coupling is probably due to the low phasemismatch between the port waveguide and the ring resonator and a relatively thin gap layer.

Simulations, however, indicate that two-ring devices can have much better performance by applying a slightly different coupling coefficient for each ring, see Fig. 6.5. Optimization of the coupling coefficients can in practice be done by applying offsets in lateral direction on the mask (see for more detail Fig. 2.3). By choosing proper device parameters a filter response as shown in Fig. 6.5 can be obtained.

Another possibility to introduce more freedom in the design is the introduction of an additional ring. As can be seen in Fig 6.6 the drop response of the three ring device with equal coupling coefficients resembles the model calculation of two ring device with individually optimized coupling coefficients, see Fig. 6.5. The response of the three-ring device has an ON-OFF

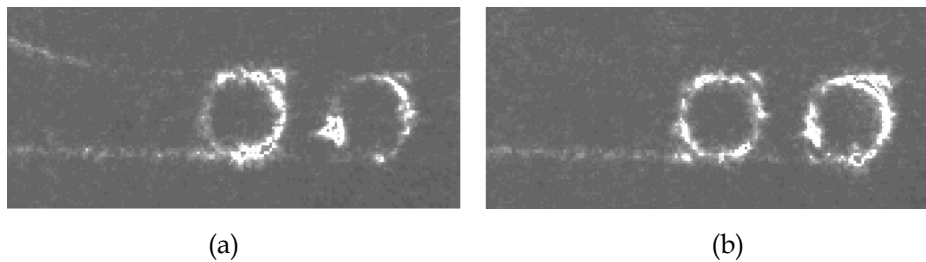


Fig. 6.7 Infra red pictures of a cascaded two-ring resonator device at the wavelength of maximum (a) and minimum (b) drop power

ratio of 20 dB and a suppression of 10 dB in agreement with the simulations. Simulations show also that by allowing a slight variation in coupling coefficients a larger suppression in the stopband can be obtained. The propagation losses in the rings obtained by our simulation model show that it has been reduced to 8 dB/cm or 0.13 dB/roundtrip. The bending loss due to radiation is estimated to be less than 1 dB/cm as calculated by Selene Stress and Temperature [C2V]. The resulting materials and scattering loss of 7 dB/cm is rather low as could be expected after the annealing step.

Fig. 6.7 shows an example of pictures taken with an IR CCD camera from the top of a two-ring device at a wavelength of maximum and minimum drop power.

These pictures confirm qualitatively the simulation model and emphasize the requirement of an appropriate optical path length to obtain the desired filter response for a certain wavelength range.

Based on promising results of cascaded two- and three-ring devices in this chapter, another ring resonator device performing as spectral slicer is presented in the following chapter.

Conclusions

Parallel cascaded ring resonator devices with improved performance such as higher ON-OFF ratio, flatter passband and faster roll-off compared with respect to single ring devices have been demonstrated. The devices with the vertical coupling configuration have been fabricated in $\text{Si}_3\text{N}_4/\text{SiO}_2$ technology and conventional optical photolithography. Their spectral response shows qualitatively the expected behavior and confirms the potential of cascaded resonator devices for WDM filter applications.

In order to be able to analyze the experimental results, a simulation model has been developed. By fitting this model to the experimental data, the physical parameters such as propagation loss inside the ring, coupling coefficients, etc. could be obtained. Alternatively the model can be used to optimize the design.

Chapter 7

Compact spectral slicer devices based on microring resonators

7.1 Introduction

After having dealt with single ring devices and higher order wavelength filters based on microring resonators, devices with a richer functionality can be treated. Within the NAIS project spectral slicers are considered that allow the generation of a number of WDM channels by a single, potentially low-cost broadband source. Instead of working with a number of relative expensive single channel laser sources at the transceiver site of an access network, a single broadband source can be used at the cost of larger complexity in the wavelength conditioning part. The proposed ultra-compact spectral slicers consist of microring resonators with slightly increasing radius to generate a series of WDM channels. The spectral efficiency of the individual channels can be substantially improved by using a cascade of identical ring resonators as higher order filter without introducing additional channel crosstalk. The detail design considerations for spectral slicer devices have been presented in [Tan 2003 (a)] and are reproduced in full in the following section. Thereafter the realization is briefly described. The experimental results are given in the third section. Finally a discussion is given.

7.2 Design of compact spectral slicers based on vertically coupled microring resonators

Conventional Wavelength Division Multiplexing (WDM) systems utilize narrowband coherent laser diodes as light source. These laser diodes are normally fabricated to be tunable over a wide range of wavelengths.

With an increasing number of WDM channels, the number of laser diodes is also increasing and consequently the costs. Especially in the access network the use of spectral slicers is an attracting low-cost alternative as they utilize a single broadband source for creating the desired WDM channels. By using spectral slicers, however, the spectral efficiency and the shape of the optical filter response becomes an issue, as the power budget in these low-cost systems without optical amplifiers is critical. In order to realize spectral slicers,

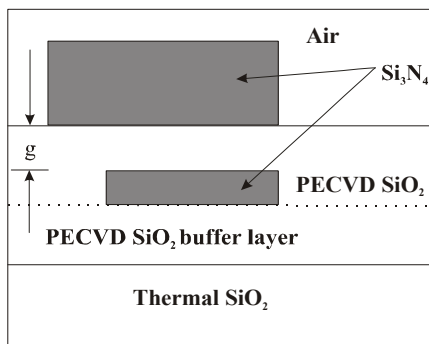


Fig. 7.1 Schematic cross-section of a vertically coupled waveguide-microring resonator

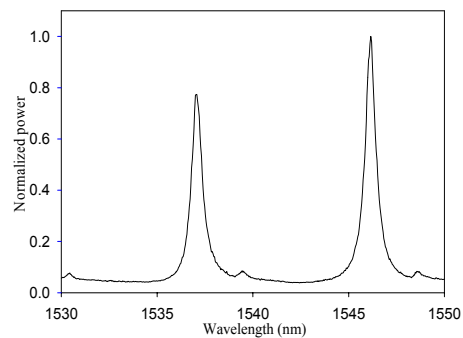


Fig. 7.2 Spectral response of the drop port of a MR with radius 25 μm

several devices such as Arrayed Waveguide Gratings (AWG) and Waveguide Grating Routers (WGR) [Jung 1998] have been demonstrated. The drawback of these devices, however, is the relatively large space needed. Microring resonators, on the other hand, offer the possibility to realize ultra-compact devices with a chip area well below 1 mm². Moreover, the spectral efficiency of the individual WDM channels can be improved by cascading several microring resonators as a higher order filter with a nearly box-car shape.

In the following a feasibility study of spectral slicers based on microring resonators is carried out in detail. In addition, a discussion is given of the influence of cascading of microring resonators for a single WDM channel on the spectral efficiency.

Vertically coupled Microring Resonators

In order to realize the spectral slicers vertically coupled microring resonators are proposed [Klunder 2001]. The cross section of the single device is given in Fig. 7.1. The straight waveguides are embedded in Plasma Enhanced Chemical Vapor Deposition (PECVD) SiO₂ and function as input and output channels.

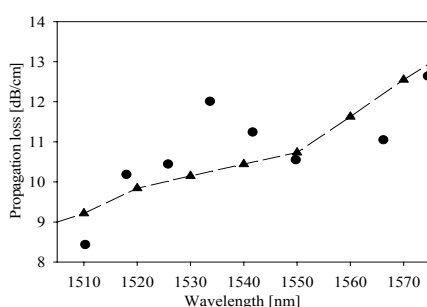


Fig. 7.3 Propagation loss in a single MR; triangles: scattering and material losses in Fig 7.4 plus calculated bending loss of the MR; dots: calculated back from the spectral responses

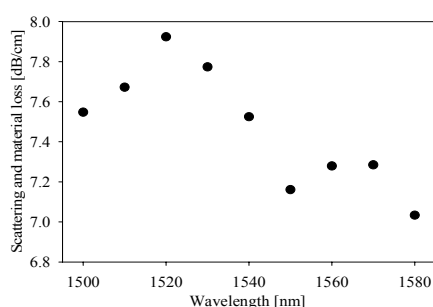


Fig. 7.4 Scattering and materials losses of waveguide channels with 1 μm width and air cladding obtained by measuring the scattered light

For an optimal technological realization a relatively thin straight waveguide core should be used to minimize overgrowing effects of the PECVD SiO₂ separation layer (g) due to the straight waveguides underneath. By using high refractive index material such as Low Pressure Chemical Vapor Deposition (LPCVD) Si₃N₄ ($n = 1.98$), the core thickness of the single mode straight waveguide with a width of 2 μm can be reduced to 140 nm. The ring resonator, also realized in Si₃N₄, has been designed such that the ring is single mode and has only a small phase mismatch with respect to the in- and output waveguides. During fabrication, Chemical Mechanical Polishing (CMP) is applied twice to remove the surface roughness of the intermediate PECVD SiO₂ layers. Fig. 7.2 shows a typical response of a single MR with 25 μm radius.

Fig. 7.3 shows the typical propagation loss of a MR as a function of wavelength determined by two ways, first the propagation loss is calculated back for each peak from the spectral responses and second the propagation loss has been calculated by using quantitative image analysis [Tan 2003 (b)]. The propagation loss increase for longer wavelengths is mainly due to the increasing bending loss of the MR. The ring resonator with the vertically coupled configuration show a relatively low off-resonance on-chip insertion loss, less than 0.1 dB [Tan 2003 (b)]. The scattering and materials loss of the in- and output waveguides is given in Fig. 7.4. The enhanced loss around 1520 nm is mainly due to the N-H overtone vibration, typically for as deposited PECVD SiON [Wörhoff 1999, Hussein 2001]. In principle, by annealing the sample at a temperature of 1150°C the maximum loss can be reduced to about 0.6 dB/cm [Hussein 2001].

Design of Spectral slicers devices

The spectral slicers are designed to be a part of a WDM transceivers for the access network as proposed in [NAIS project, Driessen 2001]. Fig. 7.5 shows

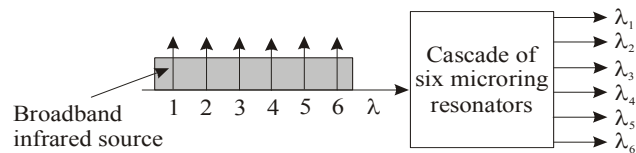


Fig. 7.5 Working principle of the microring resonators as spectral slicers with a broadband infrared source

schematically its working principle, which is similar to 1 X N WDM filter. The broadband infrared source is fed to the input port of the spectral slicer, which consists of a number of microring resonators with slightly different ring radius for selecting the desired part of the source spectrum.

The radius of the individual ring resonators (around 25 μm) is critical as an increase of 12.5 nm is sufficient to select an adjacent channel with 100 GHz channel spacing. In order to have a certain central wavelength based on the ITU grid, tuning can also be applied as demonstrated in [Geuzebroek 2002]. For tuning purposes, a cladding layer, based, for example on low-index polymers, should be applied to allow efficient local heating by electrodes on top of the ring. In the application of spectral slicers the spectral efficiency,

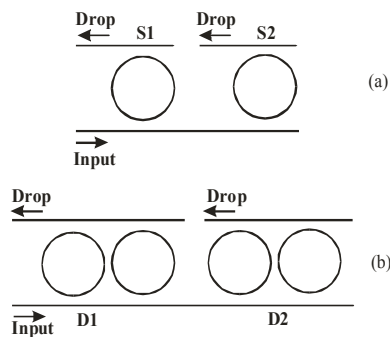


Fig. 7.6 Lay-out of a two-channel spectral slicer based on microresonators: S1: single ring resonator with radius 25 μm ; S2: single ring resonator with radius 25.0125 μm ; D1 and D2: set of ring resonators when S1 and S2 are cascaded by two identical ring resonators

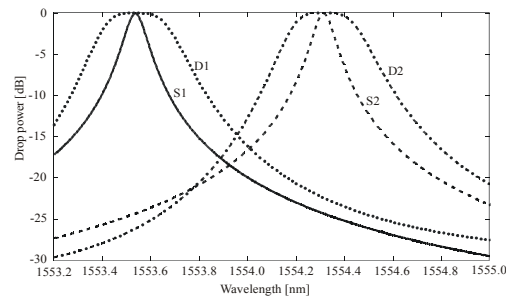


Fig. 7.7 Drop port responses of a microring resonator based two channel spectral slicer; S1 and S2 curves obtained with single ring resonator; D1 and D2 obtained with the double ring resonators, see also Fig. 7.6

which is the selected part of the power spectrum compared to the power spectrum in the same wavelength range of the source, is becoming critical. Cascading of at least two microring resonators in a single WDM channel can substantially improve the spectral efficiency. Fig. 7.6 shows schematically the layout of the spectral slicers with single ring resonator (S1 with radius 25 μm and S2 with radius 25.0125 μm) and cascade of two identical ring resonators (D1 and D2). Fig. 7.7 shows the simulation results of drop responses for a single and a cascade of two ring resonators with different ring radius.

Table 7.1 shows the parameters obtained from simulations for a two channel spectral slicer based on single or double ring resonators for each WDM channel.

	Radius (μm)	Coupling factor	α_{prop} (dB/cm)	Crosstalk (dB)	Spectral efficiency
Single ring	25 and 25.0125	0.017	2	-25	0.18
Double ring	25 and 25.0125	0.04	2	-27	0.43

Table 7.1 Summary of the parameters of a microring resonator based spectral slicer obtained by simulations

The crosstalk level of the single ring resonator response is -25 dB while for double ring resonator it is -27 dB. In order to maintain the crosstalk level at -25 dB, the spectral efficiency of the selected WDM channel is relatively low for the single microring resonator due to the Lorentzian shape of the response. Cascading of at least two microring resonators in a single device results in a box-like shape response [Geuzebroek 2002, Tan 2003 (e), Yanagase 2002], see also Fig. 7.7. By increasing the coupling factor of the double ring resonators with respect to the single ring resonator, the response of the double ring resonators can be broadened without deterioration of the crosstalk level. In this way, the spectral efficiency of the WDM channel can be improved by 240%. Considering a realistic spectral intensity of the broadband source of 1 mW/channel an estimated output power of the spectral slicer per channels is -7.4 dBm for single ring and -3.7 dBm for double rings. If the receiver sensitivity is -26 dBm then the power budget is 18.6 dB for a single ring and 22.3 dB for a double ring spectral slicer.

7.3 Realization of the spectral slicer devices

The realization of the devices (see Fig. 7.8 for a schematic layout) is based on the design of the previous section, see Fig. 7.1, but with some minor modifications. The separation layer is Tetraethylorthosilicate (TEOS) oxide with a refractive index of 1.427 instead of PECVD SiO₂. TEOS is a well known material for covering corrugated surfaces and is therefore more convenient to

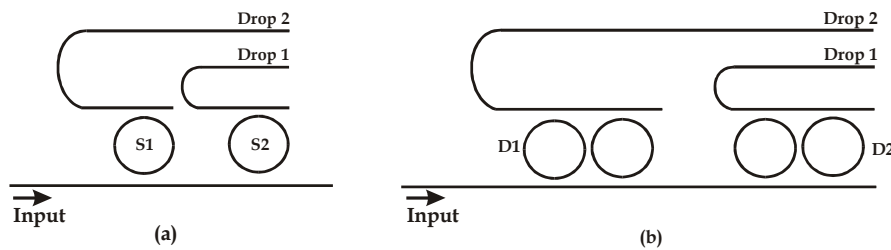


Fig. 7.8 Schematic lay out of spectral slicer device; (a) single ring device (b) cascaded two-ring device

be used as a separation layer than PECVD SiO₂. Another modification is the radius of the microring resonators, which has been reduced to 20 μm and 15 μm , in order to increase the FSR to about 10 nm and 14 nm respectively. The first set of devices are produced on the same wafer and have a ring layer of 310 nm thick LPCVD Si₃N₄ optimized for rings with a radius of 20 μm and a width of 2 μm . The microring resonator devices with a radius of 15 μm will not (yet) show optimum performance as a core thickness of 340 nm would be needed. The spectral slicer device based on microrings with a radius of about 20 μm has been designed to have a channel spacing of 3 nm, which results in an increase in the radius, ΔR of approximately 38.7 nm for each consecutive stage, both for single ring- and cascaded double rings devices.

7.4 Experimental results

The standard measurement method [Tan 2003 (b)] has been applied to characterize the devices.

End-fire coupling has been used to couple TE polarized light from a tunable laser diode to the input port of the straight waveguide. Fig. 7.9 presents the spectral response obtained from the drop port as a function of wavelength for

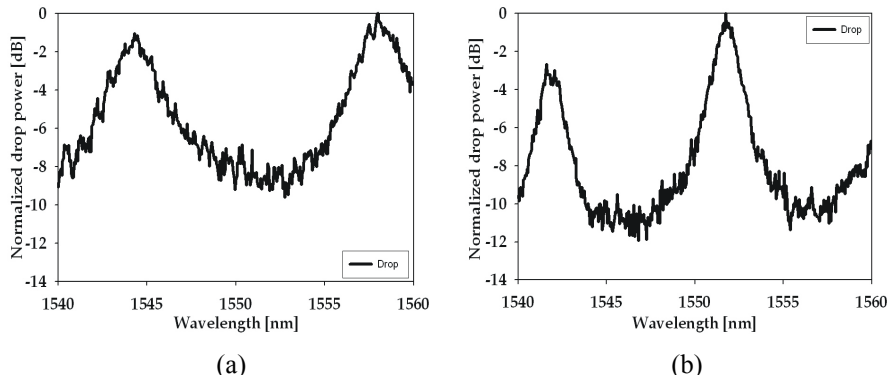


Fig. 7.9 Spectral response of a single microring resonator device with a radius of $15\ \mu\text{m}$ (a) and $20\ \mu\text{m}$ (b)

a single ring device with a radius of $15\ \mu\text{m}$ as well as $20\ \mu\text{m}$. Fig. 7.9a shows a low finesse and consequently a wide bandwidth due to the combination of the

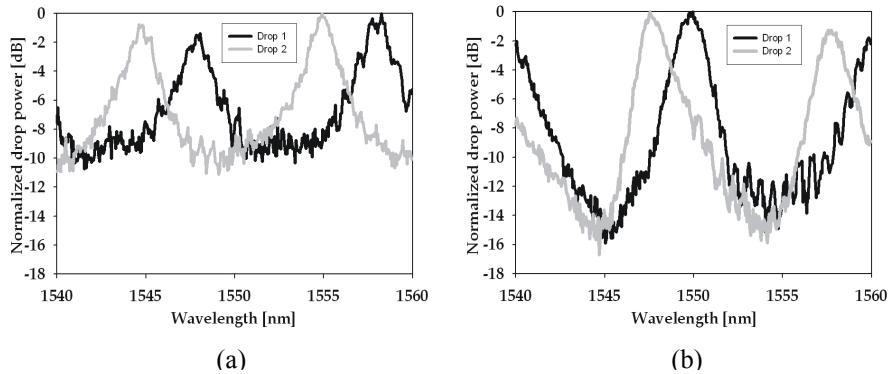


Fig. 7.10 Spectral response of spectral slicer devices based on microring resonators with a ring radius of $20\ \mu\text{m}$; (a) single ring resonator per drop channel, (b) cascaded two ring resonator per drop channel

strong coupling and high propagation loss. In Fig. 7.9b the wide bandwidth is due to the strong coupling only.

An analysis has been done for a single microring device with a radius of 15 μm and 20 μm by using the simulation model as described in Ch. 6. The propagation losses inside the microring resonator were estimated by our model to be 9 dB/cm and 35 dB/cm for a radius of 20 μm and 15 μm respectively. The field amplitude coupling coefficients are 0.73 for the ring with a radius of 15 μm and 0.65 for the ring with a radius of 20 μm . The

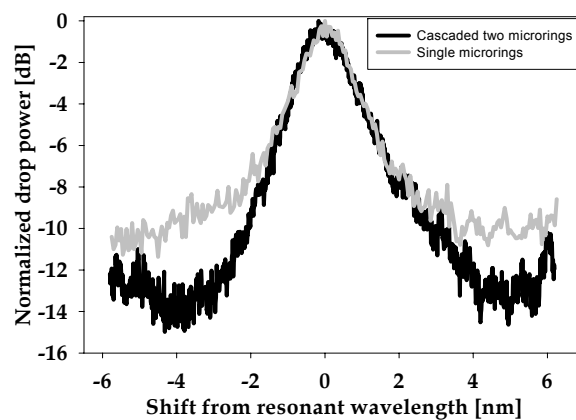


Fig. 7.11 Spectral response of the spectral slicer devices based on microring resonator with a ring radius of 20 μm ; gray curve: spectral slicer with single microring resonator; black curve: spectral slicer with cascaded two microring resonator

experimental coupling coefficients for the ring with a radius of 20 μm compare reasonably well with the numerical estimate being 0.82 as calculated with the model of Hammer [Hammer 2003]. The higher propagation loss of the microring device with a radius of 15 μm was mainly dominated by higher bending loss of about 25 dB/cm as calculated by Selene Stress and Temperature [C2V], which is due to the not optimized ring resonator core thickness. Experimental results of spectral slicer devices are given in Fig. 7.10. The expected channel spacing of about 3 nm has been closely achieved in the device consisting of a single-ring resonator stage, being 3.15 nm. For cascaded two microring resonator, this value is only slightly less, namely 2.4 nm.

This means that the ring radii are controlled within 8 nm. The crosstalk levels of the response of both devices are rather high, -9 dB and -7 dB for the single and the two ring stages respectively as the strong coupling results in broadening of the bandwidth. When correcting the response of Fig. 7.10b for the undesired shift in ring radius, the crosstalk is reduced to -11 dB. For a further reduction in crosstalk the propagation loss inside the microring should be decreased. In that case a relatively small coupling coefficient can be used that results in a narrower bandwidth. Moreover, the coupling coefficients can even more finely tuned to obtain precisely the desired response as was discussed in Ch. 6.

In order to illustrate the influence of a two-ring stage on the device performance, the resonant peak of a device with a single microring stage has been put together with the resonant peak of two ring stage (see Fig. 7.11). The cascaded two-ring resonator device shows a better rolloff ($\Delta\lambda_{-10\text{dB}}/\Delta\lambda_{-3\text{dB}}$) of about 1.28 times faster and decreased crosstalk.

The spectral efficiency (η) can be estimated by calculating $\Delta\lambda_{-3\text{dB}}$ divided by a spectral width of a single WDM channel (w) or

$$\eta = \frac{\Delta\lambda_{-3\text{dB}}}{w}$$

The measurement results in Fig. 7.11 are obtained with devices processed on the same wafer, which means the intended devices have the same coupling coefficient. In order to be able to compare the spectral efficiency we need devices with different coupling coefficients as described in the design section and shown in Table 7.1. However, a faster rolloff and lower crosstalk of the cascaded device has clearly been demonstrated.

Conclusions

Compact spectral slicer devices based on cascaded microring resonators are for the first time demonstrated.

They are realized in $\text{Si}_3\text{N}_4/\text{SiO}_2$ technology using conventional optical photolithography and employ the vertical coupling configuration. The devices with a promising performance can still be improved by tailoring the coupling coefficients, reducing the propagation loss inside the ring and by cascading more rings.

The potential of the employed technology has further been explored by reducing the ring radius and consequently enhancing the FSR. It is shown experimentally that with the $\text{Si}_3\text{N}_4/\text{SiO}_2$ technology, a FSR of 10 and 14 nm can be obtained for rings with 20 and 15 μm respectively. Comparison of resonant wavelengths of rings designed with identical ring radius reveals that the employed technology results in variations of the radius about 8 nm, i.e. less than 0.5×10^{-3} .

Chapter 8

Summary and Recommendations

8.1 Summary

This thesis describes work on microring resonator devices based on Silicon Oxynitride technology carried out in the Dutch BTS and European NAIS project. In the beginning only single ring devices have been considered in order to develop the fabrication technology as well as design and measurement methods and gain a deep understanding of the functional behavior. Later more complex devices consisting of cascaded multiple microring resonators in a parallel configuration with a promising functionality have been realized and demonstrated. In the following a summary and recommendations for future work will be given.

Chapter 1:

This chapter gives a general overview of optical communication and the possible role of microring resonator devices as optical filters for WDM systems. It describes briefly the objective of the BTS and the NAIS project and ends with a brief outline of this thesis.

Chapter 2:

General concepts of microring resonator devices are given in this chapter. The working principle of ring resonator devices and the two basic coupling schemes, lateral and vertical coupling, are described. Thereafter the performance of cascaded multiple rings in serial and parallel configuration are discussed.

Finally two characterization methods, the standard method and quantitative image analysis, are explained in detail.

Chapter 3:

A general route in order to arrive at a realistic design and to realize eventually demonstrator devices is explained in detail. A lot of constraints have a great influence on the design activities, for example the available knowledge, technological facilities and design tools, and also the objectives and time frame of the project. Several activities should be carried out such as intermediate characterizations, functional characterizations followed by system evaluations in order to end up with the final demonstrator devices.

Chapter 4:

The results obtained with microring resonator devices in the lateral coupling configuration are reported in this chapter. The Si_3N_4 based devices were analyzed in the wavelength range of 1510 to 1580 nm and a finesse of up to 182 has been achieved. The most critical issue in this configuration is the gap definition, which is rather difficult to be obtained with conventional optical photolithography.

Chapter 5:

In this chapter, work on single ring resonator devices based on SiON and Si_3N_4 in a vertical coupling configuration are presented. A feasibility study shows that it is difficult to realize single SiON microring resonator devices that can perform as polarization independent wavelength filters. Based on this experience, a polarization diversity scheme is considered and work has been focused on microring resonators optimized for TE polarization. Devices have been realized in Si_3N_4 technology, whereby a finesse of more than 100 could be demonstrated.

Chapter 6:

Increasing the complexity of devices by cascading two or three microring resonators in a parallel configuration a better performance of the filter response could be obtained. A simulation model is developed that allows the design and analysis of the multiple ring devices. Devices have been realized in Si_3N_4 technology and show a promising functionality as bandpass filter. Two-ring devices with equal coupling coefficients exhibit a rather wide passband and narrow stopband, three-ring devices show increased performance.

Chapter 7:

Another potential application of ring resonator devices, spectral slicers are presented. Devices based on microresonators with a radius of $20\ \mu\text{m}$ as well as $15\ \mu\text{m}$ have been designed and realized. A comparison is made between the performance of devices where each stage is made of either a single or a double ring configuration. The latter show much better performance with respect to faster roll-off and lower crosstalk.

Chapter 8:

This chapter presents a summary of the work described in this thesis and gives also conclusions and recommendations for future work.

8.2 Recommendations

As mentioned in the previous chapters, the performance of the filters is mainly determined by the coupling coefficients and propagation loss inside the ring resonator. Therefore simulation tools that can be used to estimate the coupling coefficients should be available. The propagation loss might be decreased by applying appropriate fabrication processes.

In the case of the lateral coupling configuration, coupling coefficients can be estimated by reducing the three-dimensional structure using an effective index method and calculate the field overlap between the mode in the port waveguide and the ring as described in [Klunder 2002 (b)]. Estimation of the coupling coefficients in three-dimensions by a simplified coupled mode theory [Hammer 2003] and semi-experimental estimations obtained by fitting the simulation model to the experimental data are in reasonable agreement (see Sec. 7.4). Fully three-dimensional coupled mode theory, however, is necessary that enable better comparison between those results and allow improved optimization of the design to obtain the desired coupling coefficients.

Developing new fabrication approaches might be useful to decrease the propagation loss inside the ring. With the currently available fabrication process the absorption and scattering loss is in the order of 6 – 8 dB/cm. An annealing process would not reduce the propagation losses significantly because the losses are mainly dominated by the scattering loss. By using a waferstepper with an overlay accuracy of about 100 nm, alignment problems between waveguide and ring mask could probably be solved. Also lower scattering loss could be expected because the roughness on the mask that is transferred directly to the photoresist in conventional optical photolithography by using contact printing will be reduced by using a projection method with size reduction. When the alignment problems have been solved, the incorporation of precise offsets in horizontal direction on the mask become useful and the coupling coefficients could be tailored more efficient to give the desired filter response.

Specific recommendations of some chapters are given in the following:

Chapter 5:

In order to be able to realize polarization independent wavelength filters, polarization diversity scheme in combination with cascading several rings can be used (see Klunder 2002 (a)).

By using this scheme, the devices need to be optimized only for a single polarization. The validity of this approach, however, should be examined by experiments.

Chapter 6:

In order to be able to have the desired filter response, the devices might be tuned e.g. thermo-optically. In the case of parallel cascaded ring devices, tuning the rings could also change the distance between centre to centre of nearest neighbor rings causing in that way an undesired filter response. Additional tuning elements located on the connecting line of the port waveguides could compensate for this effect.

Chapter 7:

Reducing the ring radius seems to cause problems to the quality of the ring layer as by increasing the layer thickness, crack can occur and bending of the wafer. In order to minimize bending of the wafer, growing a layer on both sides of the wafer might help. By applying these treatments, the layer properties such as the thickness, refractive index etc. should be carefully measured as these usually changes.

Summary and Recommendations

References

[Abeles 2000] Abeles, J.H., "Resonant enhanced modulator development", Sarnof Corporation, public release

[Albers 1995] Albers, H., Hilderink, L.T.H., Szilagyi, E., Paszti, F., Lambeck, P.V., and Popma, Th.J.A., "Reduction of hydrogen induced losses in PECVD-SiO_xN_y optical waveguide in the near infrared", in *Proc. IEEE LEOS Annual Meeting 1995*, pp. 88-89, 1995

[Absil 2000] Absil, P.P., Hryniewicz, J.V., Little, B.E., Cho, P.S., Wilson, R.A., Joneckis, L.G., and Ho, P.T., "Wavelength conversion in GaAs micro-ring resonators", *Opt. Lett.*, vol. 25, pp. 554-556, 2000

[Balistreri 2001] Balistreri, M.L.M., Klunder, D.J.W., Blom, F.C., Driessen, A., Korterik, J.P., Kuipers, L., van Hulst, N.F., "Experimental analysis of the whispering gallery modes in a cylindrical optical microresonator", *J. of Opt. Soc. Am. B*, vol. 18, pp. 465-471, 2001

[Bertolotti 2004] Bertolotti, M., Driessen, A. and Michelotti, F. (editors), "Micro resonators as Building blocks for VLSI Photonics", in *Proc. International School of Quantum Electronics, Enrice-Sicily, October 2003, AIP 2004*.

[Blom 1996] Blom, F.C., Hoekstra, H.J.W.M., Driessen, A. and Popma, Th. J.A., "A new integrated all-optical switch based on a micro-cavity", in *Proc. CLEO-Europe 1996*, pp. 20-20, Hamburg, 1996

[Blom 1997] Blom, F.C., van Dijk, D.R., Hoekstra, H.J.W.M., Driessen, A. and Popma, Th. J.A., "Experimental study of integrated optics microcavity resonators: towards and all-optical switching device", *Appl. Phys. Lett.*, vol. 71, pp. 747-749, 1997

[Blom 1998] Blom, F.C., *Linear and non-linear optical properties of cylindrical micro-resonators from materials to device realization*, Ph.D thesis 1998, University of Twente, The Netherlands

References

[Blom 1999] Blom, F.C., Kelderman, H., Hoekstra, H.J.W.M., Driessen, A., Popma, Th. J. A., Chu, S.T. and Little, B.E., "A single channel dropping filter based on a cylindrical micro-resonator", *Opt. Comm.*, vol. 167, pp. 77-82, 1999

[BTS project] Project description

[C2V] Selene Stress & Temperature and Prometheus DV, commercial product of C2V, Colosseum 20, 7521 PT Enschede, The Netherlands

[Chin 1999] Chin, M.K., Youtsey, C., Zhao, W., Pierson, T., Ren, Z., Wu, S.L., Wang, L., Zhao, Y.G., and Ho, S.T., "GaAs microcavity channel-dropping filter based on race-track resonator", *IEEE Photon. Technol. Lett.*, vol. 11, pp. 1620-1622, 1999

[Chu 1999 (a)] Chu, S.T., Pan, W., Sato, S., Kaneko, T., Little, B.E., Kokubun, Y., "Wavelength trimming of a microring resonator filter by means of a UV sensitive polymer overlay", *IEEE Photon. Technol. Lett.*, vol. 11, pp. 688-690, 1999

[Chu 1999 (b)] Chu, S.T., Little, B.E., Pan, W., Kaneko, T., Sato, S., and Kokubun, Y., "An eight-channel add-drop filter using vertically coupled microring resonators over as cross grid", *IEEE Photon. Technol. Lett.*, vol. 11, pp. 691-693, 1999

[Chu 1999 (c)] Chu, S.T., Pan, W., Suzuki, S., Little, B.E., Sato, S., and Kokubun, Y., "Temperature insensitive vertically coupled microring resonator add/drop filters by means of a polymer overlay", *IEEE Photon. Technol. Lett.*, vol. 11, pp. 1138-1140, 1999

[Chu 1999 (d)] Chu, S.T., Little, B.E., Pan, W., Kaneko, T., Kokubun, Y., "Second-order filter response from parallel coupled glass microring resonators", *IEEE. Photon. Technol. Lett.*, vol. 11, pp. 1426-1428, 1999

[Dapkus 2000] Dapkus, D., O'Brien, J., *Low voltage modulator based on semiconductor microresonators*, RFLICS kickoff meeting, public release

[Driessen 2001] Driessen, A., Geuzebroek, D.H., Klunder, D.J.W. and Tan, F.S., "Analysis of a microring resonator based ultra-compact transceiver for the access network", in *Proc. LEOS Benelux Chapter 2001*, pp. 25-28, 2001

[Driessen 2003] Driessen, A., Geuzebroek, D.H., Hoekstra, H.J.W.M., Kelderman, H., Klein, E.J., Klunder, D.J.W., Roeloffzen, C.G.H., Tan, F.S., Gersen, H.J., van Hulst, N.F., Kuipers, K, Krioukov, E., Otto, C. "Microring resonators as building blocks for VLSI photonics", accepted for publication in *American Institute of Physics (AIP) Conference Proceeding 2004*

[Geuzebroek 2002] Geuzebroek, D.H., Klein, E.J., Kelderman, H., Tan, F.S., Klunder, D.J.W. and Driessen, A., "Thermal wavelength-selective switch based on microring resonators", in *Proc. 28th European Conference on Optical Communication (ECOC)*, paper 4.2.5, Copenhagen, Denmark, 2002

[Griffel 2000] Griffel, G., "Synthesis of optical filters using ring resonator arrays", *IEEE. Photon. Technol. Lett.*, vol. 12, pp. 810-812, 2000

[Griffel 2000 (a)] Groffel, G., "Vernier effect in Asymmetrical ring resonator arrays", *IEEE. Photon. Technol. Lett.*, vol. 12, pp. 1642-1644, 2000

[Grover 2001] Grover, R., Absil, P.P., Van, V., Hryniewicz, J.V., Little, B.E., King, O., Calhoun, L.C., Johnson, F.G. and Ho, P.T., "Vertically coupled GaInAsP-InP microring resonators", *Opt. Lett.*, vol. 26, pp. 506-508, 2001

[Grover 2002] Grover, R., Van, V., Ibrahim, T.A., Absil, P.P., Calhoun, L.C., Johnson, F.G., Hryniewicz, J.V., Ho, P.T., "Parallel-cascaded semiconductor microring resonators for high-order and wide-FSR filters", *J. Lightwave Technol.*, vol. 20, pp. 872-877, 2002

[Hammer 2003] Hammer, M., *Si₃N₄ ring cavities on SiO₂- Si₃N₄- SiO₂/ TEOS support, simplified CMT model, coupling constant calculation*, NAIS internal document, Applied Analysis and Mathematical Physics (AAMP), University of Twente

References

[Heebner 2002] Heebner, J.E., Boyd, R.W., Park, Q.H., "SCISSOR solitons and other novel propagation effects in microresonator-modified waveguides", *J. Opt. Soc. Am. B.*, vol. 19, pp. 722-731, 2002

[Heimala 1996] Heimala, P., Katila, P., Aarnio, J., Heinamaki, A., "Thermally tunable integrated optical ring resonator with poly-Si thermistor", *J. Lightwave Technol.*, vol. 14, pp. 2260-2267, 1996

[Hussein 2001] Hussein, M.G., Wörhoff, K., Roeloffzen, C.G.H., Hilderink, L.T.H., de Ridder, R.M. and Driessen, A., "Characterization of thermally treated PECVD SiON layers", in *Proc. LEOS Benelux Chapter 2001*, pp. 265-268, 2001

[Ibrahim 2002] Ibrahim, T.A., Van, V., Ho, P.T., "All-optical time-division demultiplexing and spatial pulse routing with a GaAs/AlGaAs microring resonator", *Opt. Lett.*, vol. 27, pp. 803-805, 2002

[Ibrahim 2003] Ibrahim, T.A., Cao, W., Kim, Y., Li, J., Goldhar, J., Ho, P.T., Lee, C.H., "All-optical switching in a laterally coupled microring resonator by carrier injection", *IEEE. Photon. Technol. Lett.*, vol. 15, pp. 36-38, 2003

[Jung 1998] Jung, D.K., Shin, S.K., Lee, C.H., Chung, Y.C., "Wavelength-Division-Multiplexed passive optical network based on spectrum-slicing techniques", *IEEE. Photon. Technol. Lett.*, vol. 10, pp. 1334-1336, 1998

[Kapron 1980] Kapron, F.P., Keck, D.B., Maurer, R.D., "Radiation losses in glass optical waveguide", *Appl. Phys. Lett.*, vol. 17, pp. 423-425, 1980

[Klunder 2000] Klunder, D.J.W., Tan, F. S., van der Veen, T., Bulthuis, H. F., Hoekstra, H.J.W.M. and Driessen, A., "Design and characterization of waveguide-coupled cylindrical micro-ringresonator in Si₃N₄", in *Proc. LEOS Annual meeting 2000*, paper Th12, 2000

[Klunder 2000 (a)] Klunder, D.J.W., Balistreri, M.L.M., Blom, F.C., Hoekstra, H.J.W.M., Driessen, A., Kuipers, L., van Hulst, N.F., "High resolution photon scanning tunneling microscope measurements of the whispering gallery modes in a cylindrical microresonator", *IEEE. Photon. Technol. Lett.*, vol. 12, pp. 1531-1533, 2000

[Klunder 2001] Klunder, D.J.W., Krioukov, E., Tan, F.S., van der Veen, T., Bulthuis, H.F., Sengo, G., Otto, C., Hoekstra, H.J.W.M. and Driessen, A., "Vertically and laterally waveguide-coupled cylindrical microresonators in Si₃N₄ on SiO₂ technology", *Appl. Phys. B73*, pp. 603-608, 2001

[Klunder 2002 (a)] Klunder, Dion J.W., Roeloffzen, Chris G.H., Driessen, Alfred, A novel polarization-independent wavelength-division-multiplexing filter based on cylindrical microresonators, *IEEE J. Selected topics in Quantum Electronics*, vol. 8, No. 6, pp. 1294-1299, 2002

[Klunder 2002 (b)] Klunder, D.J.W., *Photon physics in integrated optics microresonators*, Ph.D thesis 2002, University of Twente, The Netherlands

[Klunder 2003] Klunder, D.J.W., Tan, F.S., van der Veen, T., Bulthuis, H.F., Sengo, G., Docter, B., Hoekstra, H.J.W.M., Driessen, A., "Experimental and numerical study of SiON microresonators with air and polymer cladding", *J. Lightwave Technol.*, vol. 21, pp. 1099-1110, 2003

[Kokubun 2002] Kokubun, Y., Kato, T., Chu, S.T., "Box-like response of microring resonator filter by stacked double-ring geometry", *IEICE Trans. Electron.*, vol. E85-C, pp. 1018-1023, 2002

[Krioukov 2002 (a)] Krioukov, E., Klunder, D.J.W., Driessen, A., Greve, J. and Otto, C., "Sensor based on an integrated optical microcavity", *Opt. Lett.*, vol. 27, pp. 512-514, 2002

[Krioukov 2002 (b)] Krioukov, E., Klunder, D.J.W., Driessen, A., Greve, J. and Otto, C., "Integrated optical microcavities for enhanced evanescent-wave spectroscopy", *Opt. Lett.*, vol. 27, pp. 1504-1506, 2002

[Krioukov 2003] Krioukov, E., Greve, J. and Otto, C., "Performance of integrated optical microcavities for refractive index and fluorescence sensing", *Sensor and Actuators B*, vol. 90, pp. 58-67, 2003

[Ladouceur 1994] Ladouceur, F., Love, J.D., Senden, T.J., "Effect of sidewall roughness in buried channel waveguide", *IEEE Proc. Optoelectron.* Vol. 141 (4), pp. 242-248, 1994

References

[Leinse 2003] Leinse, A., Driessen, A., Diemmer, M.B.J., "Electro optic modulation in a polymer ring resonator", accepted for publication in *American Institute of Physics (AIP) Conference Proceeding 2004*

[Lenz] Lenz, G., Madsen, C.K., *Advanced microring resonator filter technology*, Lucent Technologies, public release

[Levi 1993] Levi, A.F.J., Slusher, R.E., Mc. Call, S.L., Glass, J.L., Pearton, S.J. and Logan, R.A., "Directional light coupling from microdisk laser", *Appl. Phys. Lett.*, vol. 62, pp. 561-563, 1993

[Little 1997] Little, B.E., Chu, S.T., Haus, H.A., Foresi, J. and Laine, J.P., "Microring resonator channel dropping filters", *J. Lightwave Technol.*, vol. 15, pp. 998-1005, 1997

[Little 1998] Little, B.E., Haus, H.A., Foresi, J.S., Kimerling, L.C., Ippen, E.P., and Ripin, D.J., "Wavelength switching and routing using absorption and resonance", *IEEE Photon. Technol. Lett.*, vol. 10, pp. 816-818, 1998

[Little 1999] Little, B.E., Chu, S.T., Pan, W., Ripin, D., Kaneko, T., Kokubun, Y., Ippen, E., "Vertically coupled glass microring resonator channel dropping filters", *IEEE Photon. Technol. Lett.*, vol. 11, pp. 215-217, 1999

[Little 2000 (a)] Little, B.E., Chu, S. T., Pan, W. and Kokubun, Y., "Microring resonators arrays for VLSI photonics", *IEEE Photon. Technol. Lett.*, vol. 12, pp. 323-325, 2000

[Little 2000 (b)] Little, B.E., Chu, S.T., Hryniewicz, J.V., Absil, P.P., "Filter synthesis for periodically coupled microring resonators", *Opt. Lett.*, vol. 25, pp. 344-346, 2000

[Little 2003] Little Optics, Inc., www.littleoptics.com

[Ma 2001] Ma, Y., Chang, S.H., Chang, S.S., Ho, S.T., "Improved optical filter responses in cascaded InGaAsP/InP microdisk resonators", *Elect. Lett.*, vol. 37 (9), 2001

- [Madsen 1999] Madsen, C.K., Zhao, J.H., *Optical filter design and analysis: a signal processing approach*, John Wiley & Sons, Inc. 1999
- [Maiman 1960] Maiman, T.H., "Stimulated optical radiation in ruby", *Nature*, vol. 187, pp. 493-494, 1960
- [Melloni 2001] Melloni, A., "Synthesis of parallel-coupled ring resonator filter", *Opt. Lett.*, vol. 26, pp. 917-919, 2001
- [Melloni 2003] Melloni, A., Costa, R., Monguzzi, P., Martinelli, M., "Ring-resonator filters in silicon oxynitride technology for dense wavelength-division multiplexing systems", *Opt. Lett.*, vol. 28, pp. 1567-1569, 2003
- [NAIS project] Project description
- [NAIS Website] www.mesap.us.utwente.nl/nais with subdirectory 2003 meetings, 39th International School of Quantum Electronics and follows the link
- [Orta 1995] Orta, R., Savi, P., Tascone, R., Trincherio, D., "Synthesis of multiple-ring-resonator filters for optical systems", *IEEE Photon. Technol. Lett.*, vol. 7, pp. 1447-1449, 1995
- [Rabiei 2002] Rabiei, P., Steier, W.H., Zhang, C., Dalton, L.R., "Polymer micro-ring filters and modulators", *J. Lightwave Technol.*, vol. 20, pp. 1968-1975, 2002
- [Rabus 2001] Rabus, D.G., Hamacher, M., "MMI-coupled ring resonators in GaInAsP-InP", *IEEE Photon. Technol. Lett.*, vol. 13, pp. 812-814, 2001
- [Rabus 2002] Rabus, D.G., Hamacher, M., Troppenz, U., Heidrich, H., "Optical filters based on ring resonators with integrated semiconductor optical amplifiers in GaInAsP-InP", *IEEE J. Selected topics in Quantum Electronics*, vol. 8, No. 6, pp. 1405-1411, 2002
- [Roeloffzen 2002] Roeloffzen, C.G.H., *Passband flattened binary-tree structured add-drop multiplexers using SiON waveguide technology*, Ph.D thesis 2002, University of Twente, The Netherlands

References

[Smit 1996] Smit, M.K., van Dam, Cor, "Phasar-based WDM-devices: principle, design and applications", *IEEE J. Selected topics in Quantum Electronics*, vol. 2, No. 2, pp. 236-250, 1996

[Suzuki 2002] Suzuki, S., Hatakeyama, Y., Kokubun, Y., Chu, S.T., "Precise control of wavelength channel spacing of microring resonator add-drop filter array", *J. Lightwave Technol.*, vol. 20, pp. 745-750, 2002

[Tan 2001 (a)] Tan, F.S., Klunder, D.J.W., Bulthuis, H.F., Sengo, G., Hoekstra, H.J.W.M. and Driessen, A., "High finesse micro-ring resonator for WDM applications", in *Proc. 10th of ECIO 2001*, pp. 489-492, 2001

[Tan 2001 (b)] Tan, F.S., Klunder, D.J.W., Bulthuis, H.F., Sengo, G., Hoekstra, H.J.W.M. and Driessen, A., "Direct measurement of the on-chip insertion loss of high finesse microring resonators in Si₃N₄-SiO₂ technology", in *Proc. LEOS Benelux Chapter 2001*, pp. 181- 184, 2001

[Tan 2002 (a)] Tan, F.S., Klunder, D.J.W., Kelderman, H., Hoekstra, H.J.W.M. and Driessen, A., "High finesse vertically coupled waveguide-microring resonators based on Si₃N₄-SiO₂ technology", in *Proc. Workshop on Fibers and Optical Passive Components (WFOPC)*, pp. 228-232, Glasgow, Scotland, 2002

[Tan/Klunder 2002] Modification of simulation model of through port analysis to be used for drop port analysis of multimodal single microring resonator, unpublished

[Tan 2003 (a)] Tan, F.S., Geuzebroek, D.H. and Driessen, A., "Design of compact spectral slicers based on vertically coupled microring resonators", in *Proc. 11th European Conference on Integrated Optics (ECIO)*, pp. 363-366, Prague, Czech Republic, 2003

[Tan 2003 (b)] Tan, F.S., Klunder, D.J.W., Sengo, G., Kelderman, H., Hollink, A., Hoekstra, H.J.W.M., Driessen, A., "Characterization of vertically waveguide coupled microring resonators by means of quantitative image analysis", *Journal of Nonlinear Optical Physics and Materials*, vol. 12, No. 2, pp. 205-212, 2003

[Tan 2003 (c)] Simulation model for drop port analysis of single microring resonator, unpublished

[Tan 2003 (d)] Simulation model for drop port analysis of multiple microring resonators, unpublished

[Tan 2003 (e)] Tan, F.S., Kelderman, H. and Driessen, A., "High ON-OFF ratio of cascaded two and three microring resonators based on SiON technology for bandpass filter applications", in *Proc. 29th European Conference on Optical Communication (ECOC)*, paper We 1.2.5, pp. 364-365, Rimini, Italy, 2003

[Van 2002 (a)] Van, V., Ibrahim, T.A., Ritter, K., Absil, P.P., Johnson, F.G., Grover, R., Goldhar, J., Ho, P.T., "All-optical Nonlinear switching in GaAs-AlGaAs Microring Resonators", *IEEE J. Selected topics in Quantum Electronics*, vol. 8, No. 3, pp. 705-713, 2002

[Van 2002 (b)] Van, V., Ibrahim, T.A., Absil, P.P., Johnson, F.G., Grover, Ho, P.T., "Optical signal processing using Nonlinear semiconductor microring resonators", *IEEE Photon. Technol. Lett.*, vol. 14, pp. 74-76, 2002

[Wörhoff 1996] Wörhoff, K., *Optimized LPCVD SiO_xN_y waveguides covered with calixarene for non-critically phase-matched second harmonic generation*, Ph.D thesis 1996, University of Twente, The Netherlands

[Wörhoff 1999] Wörhoff, K., Lambeck, Paul V. and Driessen, Alfred, "Design, Tolerance Analysis, and fabrication of silicon oxynitride based planar optical waveguides for communication devices", *J. Lightw. Techn.*, vol. 17, pp. 1401-1407, 1999

[Wörhoff 2002] Wörhoff, K., Hilderink, L.T.H., Driessen, A., Lambeck, P. V., "Silicon oxynitride: a versatile material for integrated optics application", *J. Electrochemical Society*, vol. 149, pp. 85-91, 2002

[Yanagase 2002] Yanagase, Y., Suzuki, S., Kokubun, Y., Chu, S.T., "Box-like filter response and expansion of FSR by a vertically triple coupled microring resonator filter", *J. Lightwave Technol.*, vol. 1, pp. 1-5, Jan 2002

References

Publications

Publications in peer reviewed journal

[1] **Tan, F.S.**, Klunder, D.J.W., Geuzebroek, D.H., Sengo, G., Kelderman, H., Hoekstra, H.J.W.M. and Driessen, A. (2003). "Characterization of vertically coupled waveguide-microring resonators by means of quantitative image analysis". *Journal of Nonlinear Optical Physics and Materials*, 12 (2), pp. 205-212. ISSN 0218-8635

[2] Klunder, D.J.W., **Tan, F.S.**, van der Veen, T., Bulthuis, H.F., Sengo, G., Docter, B., Hoekstra, H.J.W.M. and Driessen, A. (2003). "Experimental and numerical study of SiON microresonators with air and polymer cladding". *IEEE J. Lightwave Technol.*, 21 (4), pp. 1099-1110. ISSN 0733-8724

[3] Klunder, D.J.W., Krioukov, E., **Tan, F.S.**, van der Veen, T., Bulthuis, H.F., Sengo, G., Otto, C., Hoekstra, H.J.W.M. and Driessen, A. (2001). "Vertically and laterally waveguide-coupled cylindrical microresonators in Si₃N₄ on SiO₂ technology". *Appl. Phys. B*, 73, pp. 603-608. ISSN 0946-2171

[4] Driessen, A., Hoekstra, H.J.W.M., Klunder, D.J.W., **Tan, F.S.**, "Fundamental lower size limit in wavelength selective structures", submitted to *Physical Review A*

Publications in reviewed conference proceedings

[1] **Tan, F.S.**, Kelderman, H., Driessen, A. "Bandpass filter based on parallel cascaded multiple microring resonators", accepted for publication in *American Institute of Physics (AIP) Conference Proceeding 2004*

[2] Driessen, A, Geuzebroek, D.H., Hoekstra, H.J.W.M., Kelderman, H., Klein, E.J., Klunder, D.J.W., Roeloffzen, C.G.H., **Tan, F.S.**, Gersen, H.J., van Hulst, N.F., Kuipers, K, Krioukov, E., Otto, C. "Microring resonators as building blocks for VLSI photonics", accepted for publication in *American Institute of Physics (AIP) Conference Proceeding 2004*

[3] **Tan, F.S.**, Kelderman, H., Driessen, A. (2003, September 21-25). "High ON-OFF ratio of cascaded two and three microring resonators based on SiON technology for bandpass filter applications", *proceedings of the 29th European Conference on Optical Communication*. paper We 1.2.5. (pp. 364-365). Rimini, Italy.

[4] **Tan, F.S.**, Geuzebroek, D.H. and Driessen, A. (2003, April 2-4). "Design of compact spectral slicers based on vertically coupled microring resonators", *proceedings of the 11th European Conference on Integrated Optics*. (pp. 363-366). Prague, Czech Republic. ISBN 80-01-02729-5

[5] Geuzebroek, D.H., Klein, E.J., Kelderman, H., **Tan, F.S.**, Klunder, D.J.W., Driessen, A. (2002, December 9). "Thermal Tuneable, Wide FSR Switch based on Micro-ring Resonators", *proceedings of IEEE/LEOS Benelux Chapter*. (pp. 155-158). Amsterdam, The Netherlands. ISBN 90-8077519-1-X

[6] Geuzebroek, D.H., Klein, E.J., Kelderman, H., **Tan, F.S.**, Klunder, D.J.W., Driessen, A., (2002, September 8-12). "Thermal Wavelength-selective Switch Based on Micro-ring Resonators", *proceedings of the 28th European Conference on Optical Communication*. (paper 4.2.5). Copenhagen, Denmark

[7] **Tan, F.S.**, Klunder, D.J.W., Kelderman, H., Hoekstra, H.J.W.M. and Driessen, A. (2002, June 5-6). "High finesse vertically coupled waveguide-microring resonators based on Si₃N₄-SiO₂ technology", *proceedings of the Workshop on Fiber and Optical Passive Components*. (pp. 228-232). Glasgow, Scotland. ISBN 0-7803-7556-4

[8] **Tan, F.S.**, Klunder, D.J.W., Bulthuis, H.F., Sengo, G., Hoekstra, H.J.W.M., and Driessen, A. (2001, December 3). "Direct measurement of the on-chip insertion loss of high finesse microring resonators in Si₃N₄-SiO₂ technology". *proceedings IEEE/LEOS Benelux Chapter*. (pp. 181-184). Brussels, Belgium. ISBN 90-5487247-0

[9] Driessen, A., Geuzebroek, D.H., Klunder, D.J.W., **Tan, F.S.** (2001, December 3). "Analysis of a microring resonator based ultra-compact transceiver for the access network". *proceedings IEEE/LEOS Benelux Chapter*. (pp. 25-28). Brussels, Belgium. ISBN 90-5487247-0

[10] Klunder, D.J.W., Kremer, J., **Tan, F.S.**, Sengo, G., Krioukov, E., Otto, C., Hoekstra, H.J.W.M., & Driessen, A. (2001, December). "All-optical switching devices in integrated optics cylindrical microresonators (an experimental feasibility study)". *proceedings of third annual meeting of the COST action P2; Nonlinear Optics for the Information Society*. (pp. 57-62). Kluwer Academic Publishers, Dordrecht, The Netherlands. ISBN 1-4020-0132-0

[11] Klunder, D.J.W., **Tan, F.S.**, Veen, T. van der, Bulthuis, H.F., Sengo, G., Hoekstra, H.J.W.M., & A. Driessen, (2001, November). "Minimized losses in a cylindrical microresonator by use of a cladding: experimental and numerical study". *proceedings of the 14th annual meeting of IEEE LEOS*. (pp. 582-583). San Diego, USA. ISSN 1092-8081

[12] **Tan, F.S.**, Klunder, D.J.W., Bulthuis, H.F., Sengo, G., Hoekstra, H.J.W.M., and Driessen, A. (2001, April 4-6). "High finesse micro-ringresonator for WDM applications". *proceedings 10th European Conference on Integrated Optics*. (pp. 489-492). Paderborn, Germany. ISBN 3-00-007634-4

[13] Klunder, D.J.W., **Tan, F.S.**, Krioukov, E., Veen, T. van der., Bulthuis, H.F., Sengo, G., Otto, C., Hoekstra, H.J.W.M., and Driessen, A. (2001, April 4-6). "New developments in high finesse integrated optics waveguide-coupled cylindrical microresonators in Si₃N₄ on SiO₂ technology". *proceedings 10th European Conference on Integrated Optics*. (pp. 485-488). Paderborn, Germany. ISBN 3-00-007634-4

[14] Klunder, D.J.W., **Tan, F.S.**, Veen, T. van der., Bulthuis, H.F., Hoekstra, H.J.W.M., Driessen, A. (2000, November 13-16). "Design and characterization of waveguide-coupled cylindrical microring resonators in Si₃N₄". *proceedings of 13th annual meeting of IEEE Laser and Electro-Optics Society (LEOS)*. (pp. 758-759). Puerto Rico, USA. ISSN 1092-8081

Presentations

[1] **Tan, F.S.**, Klunder, D.J.W., Kelderman, H., Hoekstra, H.J.W.M. and Driessen, A., (2002, October 3). *High finesse vertically coupled waveguide-microring resonators based on Si₃N₄-SiO₂ technology*, [poster presentation at MESA+ meeting], Enschede, The Netherlands

[2] Michelotti, F., Gniewek, A., Giorgi, R., Bertolotti, M., Klunder, D.J.W., **Tan, F. S.**, Driessen, A. (2002, September 30-October 8). *Principle of operation of ring microresonator devices*. [oral presentation, INFM School on Progress in Laser Sources and Photonic Devices]. Capri, Italy

[3] **Tan, F.S.**, Klunder, D.J.W., Geuzebroek, D.H., Sengo, G., Kelderman, H., Hoekstra, H.J.W.M. and Driessen, A. (2002, July 3-5). *Characterization of vertically coupled waveguide-microring resonators by means of quantitative image analysis*. [oral presentation, 2nd International Symposium on Modern Optics and Its Applications]. Bandung Institute of Technology, Bandung, Indonesia

[4] Michelotti, F., Gniewek, A., Giorgi, R., Klunder, D.J.W., **Tan, F. S.**, Driessen, A. and Bertolotti, M. (2002, May 30). *Integrated optical systems based on ring microresonators*. [oral presentation, 3rd Italian Conference on Diffractive Optics and Microstructures]. Montecatini Terme, Italy

[5] Klunder, D.J.W., Krioukov, E., Kuiper, V.S., **Tan, F.S.**, Stouwdam, W., Sengo, G., Hoekstra, H.J.W.M., Veggel, F.C.J.M. van, Otto, C., & Driessen, A., (2001, December 19). *All-optical switching and stimulated emission in high-Q microresonators* [Posterpresentatie wetenschappelijke vergadering FOM-GM], Veldhoven, The Netherlands

[6] Bostan, C.G., Klunder, D.J.W., Sengo, G., Stoffer, R., **Tan, F.S.**, Driessen, A., Hoekstra, H.J.W.M., Lambeck, P.V., Ridder, R.M. de., Wörhoff, K. (2001, October 11). *Towards ultra-compact integrated optics devices*, [poster presentation at MESA+ meeting], Hengelo, The Netherlands

[7] Klunder, D.J.W., Krioukov, E., **Tan, F.S.**, Veen, T. van der, Kremer, J., Bulthuis, H.F., Hoekstra, H.J.W.M., Otto, C., & Driessen, A. (2001, June 26). *Experimental feasibility study of all-optical switching devices in cylindrical microresonators.*, [poster presentation FOM, Photon Physics in Optical Materials], Amsterdam, The Netherlands

[8] Klunder, D.J.W., **Tan, F.S.**, Krioukov, E., Veen, T. van der., Bulthuis, H.F., Sengo, G., Otto, C., Hoekstra, H.J.W.M., and Driessen, A. (2001, April 4-6). *New developments in high finesse integrated optics waveguide-coupled cylindrical microresonators in Si₃N₄ on SiO₂ technology.*, [invited talk on 10th European Conference on Integrated Optics]. Paderborn, Germany

Acknowledgment

This thesis consists of the results of four years research in the Integrated Optical MicroSystem (IOMS) Group, MESA⁺ Research Institute, Faculty of Electrical Engineering, Mathematics and Computer Science, University of Twente. With the completion of this thesis, I would like to take this opportunity to thank everybody with whom I had discussion, 'samenwerking' and support.

First, I would like to thank my promoter Alfred Driessen for his critical comments and his patience in reading the draft of my thesis. Also for the opportunity to work within the BTS project ringresonatoren and the European Commission funded IST project Next-generation Active Integrated-optics Subsystems (NAIS). I would like also to thank the promotion committee: H.W.M Salemink, M.O.Tjia, W. van Etten, E. van Groesen, P.V. Lambeck and W.H.M. Zijm.

Within the BTS project, I would like to thank Henk Bulthuis and Dion Klunder for discussion in the single ring resonator devices, Lucie Hilderink for some information on deposition process and layer depositions of my first test devices, Meindert Dijkstra for doing CMP of my PECVD SiO₂ layer, Robert Wijn for dicing work of my first devices and Gabriel Sengo for etching work of my first test devices. In the NAIS project, I would like to thank Henry Kelderman for discussions about devices fabrication and mask design. He also fabricated my devices. Mart Diemeer for some information on polymer, Douwe Geuzebroek for discussions on cascading devices and system aspects, Arne Leinse for discussions about polymer ring resonators and Edwin Klein for discussions on the mask design. I would like to thank Anton Hollink for technical support, especially when my computer was restarting by itself and Henk van Wolferen with his help for making the experimental set-up works properly. Special thanks to Geert Altena for recovering my data from the semi-damage hard disk.

Acknowledgement

Thanks are also to Kerstin Wörhoff for information on fabrication process, Cazimir Bostan for some helps in making SEM pictures and discussions some other interesting matters and Gammar Hussein for some PECVD information.

My work at the IOMS group has been enjoyable with the interaction with Hugo Hoekstra, Rene de Ridder, Joris van Lith, Ronald Dekker and Wico Hopman. Also Rita ter Weele for very good administration supports. I would like also to thank Indonesian people, Alexander Iskandar, David Marpaung, Didit Yudistira, Hardian Suprpto, Henri Uranus, Herman, Rachmat Hidayat, and Yahya for the sharing we have done during lunch time. Thank to Universitas Katolik Parahyangan for permission to leave my work during my Ph.D study.

Finally, I would like to thank my parent and family for their supports, also my wife, Dorothy Nancy, who always supports me and was willing to cross the world with me. My daughter, Amadea Constantine and my son, Hansel Christopher, I promise I will have more time to play with you after I completed this work.

February 2004

Curriculum Vitae

Freddy Susanto Tan was born in Bandung, Indonesia on 24 November 1966. After he completed his high school at Sekolah Menengah Atas Kristen (SMAK) 2 in Bandung, Indonesia he started to study Physics at the Institut Teknologi Bandung (ITB), Indonesia in 1986. He completed his Bachelor in 1992, after which he worked as a teaching assistant there for one and half year at the Universitas Katolik Parahyangan (Unpar) in Bandung. In 1993 he became a permanent staff at the Physics Department, Faculty of Mathematics and Natural Sciences (FMIPA), Universitas Katolik Parahyangan. In 1995 he started his Master study in Physics at ITB and he completed his Master in 1998. In March 1999 he became a Research Fellow at the Integrated Optical MicroSystem (IOMS) Group (formerly Lightwave Devices Group), Faculty of Electrical Engineering, Mathematics, and Computer Science, MESA⁺ Research Institute, University of Twente. Since December 1999 he has become a Ph.D. student at the same group. He completed his Ph.D on 20 February 2004.